EFFECT OF FIBRE REINFORCEMENT ON THE CRACK PROPAGATION IN CONCRETE

by

ANTHONY SZE-TONG YAM

B.Sc., The University of Saskatchewan,1979

A THESIS SUBMITTED IN PARTIAL FULFILMENT OF
THE REQUIREMENTS FOR THE DEGREE OF
MASTER OF APPLIED SCIENCE

in

THE FACULTY OF GRADUATE STUDIES

(Department of Civil Engineering)

We accept this thesis as conforming
to the required standard

THE UNIVERSITY OF BRITISH COLUMBIA

July 1981

In presenting this thesis in partial fulfilment of the requirements for an advanced degree at the University of British Columbia, I agree that the Library shall make it freely available for reference and study. I further agree that permission for extensive copying of this thesis for scholarly purposes may be granted by the head of my department or by his or her representatives. It is understood that copying or publication of this thesis for financial gain shall not be allowed without my written permission.

Department of Civil Engineering

The University of British Columbia
2075 Wesbrook Place
Vancouver, Canada
V6T 1W5

Date July 24, 1981

ABSTRACT

The influence of fibre reinforcement on crack propagation in concrete was studied. Thirty-five double torsion specimens, made with three types of fibres (fibreglass, straight steel fibres and deformed steel fibres) were tested. The variables were the fibre volume and size of the fibres. The test results indicated that the resistance to rapid crack growth increased somewhat with increasing fibre content up to about 1.25% - 1.5% by volume. The degree of compaction had an enormous effect on the fracture properties. The fracture toughness increased with fibre content up to about 1.25% by volume, and then decreased, due to incomplete compaction. It was found that in this test geometry, fibres did not significantly restrain crack growth. It was also observed that once the crack had propagated down the full length of the specimen, the system changed from a continuous system to a discontinuous system, consisting of two separate plates held together by the fibre reinforcement. Different types of fibres did not significantly affect the fracture toughness.

ACKNOWLEDGEMENTS

The author expresses his indebtedness to Professors S. Mindess and J.S. Nadeau for their valuable guidance in planning and carrying out the investigation. The author is grateful to Professor R.J. Gray for his advice. The author also wishes to thank the Civil Engineering Department technicians and especially Mr. B. Merklie for his assistance in making the test equipment and carrying out the test.

This research was made possible by grants from the National Sciences and Engineering Research Council Canada, and the Natural, Applied and Health Sciences Grants Committee, U.B.C.

TABLE OF CONTENTS

LIST OF FIGURES

LIST OF TABLES

LIST OF SYMBOLS

a	length of the sèmi-major axis, or one half of the crack length
a_e	effective crack length
B	slope of the V-K_I curve
b_o	interatomic equilibrium bond spacing (lattice spacing)
C	system compliance
c	the y-intercept of the V-K_I curve
E	modulus of elasticity
G	energy release rate
G_{IC}	critical strain energy release rate
K_I	stress intensity factor, where subscript I refers to Mode I failure
K_{IC}	critical stress intensity factor (also known as fracture toughness)
lbf	pound force
P	applied load
r,θ	corresponding polar coordinates
t	thickness of the double torsion specimen
t_n	plate thickness in the plane of the crack
V	crack velocity
W	width of the double torsion specimen
xx,yy	cartesian coordinates with the origin at the crack tip
y	deflection
γ	surface tension
ν	Poisson's ratio
ρ	radius of curvature at the tip of the ellipse
σ	applied stress
σ_{aa}	resultant stress in a-a direction, subscript aa represents the direction
σ_m	ideal fracture strength
σ_y	yield strength
ω_m	moment arm

Chapter I

INTRODUCTION

Concrete and related cementitious materials are heterogeneous and composite in nature. Microcracks are an inherent characteristic of such materials, due to volume changes of the cement paste during hydration and due to shrinkage of the hardened cement paste upon drying. When under load, these microcracks will extend, forming an extensive crack network which eventually leads to one or more large cracks and subsequent failure.

Control of cracking is particularly important for the serviceability of reinforced concrete structures. Adequate crack control often can be achieved using smaller reinforcement bars, more closely spaced. Results have shown that concrete structures with fibre reinforcement develop finer cracks under loading. Yet, how do fibres work? Do they act as crack arrestors or do they simply hold the cracked structure together? If the fibres do arrest cracks, then how do they affect the crack growth rate?

One means of gaining an understanding of these phenomena is through fracture mechanics. Using this approach, the fracture strength, σ_f, is inversely proportional to the square root of the size of the critical flaw. When a stress less than σ_f is applied, the structure will support that stress only as long as the flaw does not grow to the critical size for that stress. Research on brittle materials has shown

that flaws will grow under sustained loading - a phenomenon known as subcritical crack growth. Subcritical crack propagation is caused by localized crack tip stresses, which are directly related to the stress intensity factor K_I. Thus crack growth can be expressed as a function of the stress intensity factor. The relationship between crack growth and the stress intensity factor can best be described by a $V-K_I$ plot, i.e. a plot of crack velocity vs stress intensity. Once the crack growth has been characterized in this way, design criteria can be developed for such a material, and a better understanding of the mechanisms governing crack growth can often be obtained. In addition, the life expectancy of structural elements made with such materials can then be predicted.

The objectives of the research reported here were:

1. To investigate the effect of fibre reinforcement on crack growth in concrete.
2. To determine quantitatively the effect of fibre content on the fracture toughness of concrete.

Chapter 2

FRACTURE MECHANICS: GENERAL BACKGROUND

2.1 Historical Background

Stresses around cracks have been studied in detail by many people. In 1913, Inglis[1a] showed that stresses around an elliptical hole (an ellipse is often used to characterize the general geometry of a crack) in a uniformly stressed plate could be expressed as

$$\sigma_{aa} = \sigma\left(1 + 2\sqrt{\frac{a}{\rho}}\right) \tag{1}$$

where σ_{aa} = resultant stress in a-a direction

σ = applied stress

a = length of the semi-major axis, or one-half of the crack length

ρ = radius of curvature at the tip of the ellipse

Westergaard[2] showed that stresses near a sharp crack could be expressed as

$$\sigma_{xx} = \sigma\sqrt{\frac{a}{2r}}\cos\frac{\theta}{2}\left(1 - \sin\frac{\theta}{2}\sin\frac{3\theta}{2}\right) + \cdots \tag{2}$$

$$\sigma_{yy} = \sigma\sqrt{\frac{a}{2r}}\cos\frac{\theta}{2}\left(1 - \sin\frac{\theta}{2}\sin\frac{3\theta}{2}\right) + \cdots \tag{3}$$

$$\sigma_{xy} = \sigma\sqrt{\frac{a}{2r}}\sin\frac{\theta}{2}\cos\frac{\theta}{2}\cos\frac{3\theta}{2} + \cdots \tag{4}$$

---

[a]numbers refer to bibliography at the end

where: subscripts xx, yy and xy represent the coordinate directions

xx and yy = Cartesian coordinates with the origin at the crack tip

r,θ = corresponding polar coordinates

and the other symbols are as defined above.

These crack tip coordinates are shown in Figure 2.1. With the help of these solutions, the theory of the mechanics of fracture can be developed.

The tensile strength of an ideal crystalline body is the stress which must be applied to cause it to fracture across a particular crystallographic plane. This ideal strength can be expressed as (3)

$$\sigma_m = \sqrt{\frac{E\gamma}{b_o}} \tag{5}$$

where σ_m = ideal fracture strength

E = modulus of elasticity

γ = surface tension

b_o = interatomic equilibrium bond spacing (lattice spacing)

If we modify the Inglis solution (Eq. 1) by equating $\rho = b_o$, and also note that $2\sqrt{\frac{a}{b_o}} >> 1$, we obtain

$$\sigma_{aa} = 2\sigma\sqrt{\frac{a}{b_o}} \tag{6}$$

Figure 2.1 Crack Front Coordinates

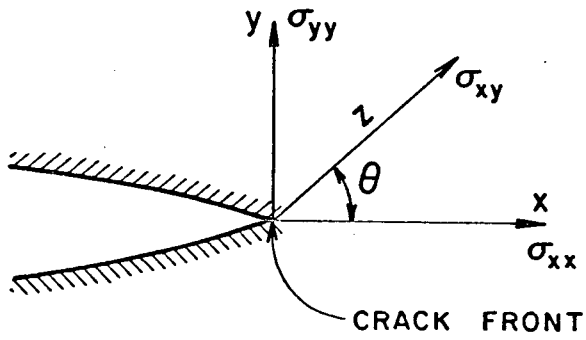

By letting the aa direction be the xx direction, then

$$\sigma_{aa} = \sigma_{xx} = 2\sigma\sqrt{\frac{a}{b_o}} \tag{7}$$

Using this modified form and equating $\sigma_{xx} = \sigma_m$ as a fracture criterion, at fracture $\sigma = \sigma_F$. Hence

$$\sigma_F = \sqrt{\frac{E\gamma}{4a}} \tag{8}$$

Thus, the fracture strength is inversely related to the square root of the length of the crack.

In 1920, based on tests on precracked glass specimens, Griffith[4] concluded that "for an infinitesimally small amount of crack extension, the decrease in stored elastic energy of a cracked body under fixed grip conditions is identical to the decrease in potential energy under conditions of constant loading". Griffith showed that the driving force for crack extension was the difference between the energy which could be released if the crack was extended and that needed to create new surfaces. Using an energy-rate balance approach, he showed that

$$\sigma_F = \sqrt{\frac{2E\gamma}{\pi a}} \qquad \text{(plane stress)} \tag{9}$$

which is very similar to Eq.8, even though they were derived from different considerations. By defining the energy release rate (crack driving force) as G, and noting that this crack driving force equals the surface energy of the newly formed surface, 2γ, (two new surfaces are created due to cracking),

it can be concluded that

$$G = 2\gamma \tag{10}$$

and

$$\sigma_F = \sqrt{\frac{EG}{\pi a}} \tag{11}$$

Griffith's approach provided the basis for the concept of treating fracture in terms of the change in energy remote from the immediate atomic environment of the crack tip. One drawback of his theory was that it was based on an ideally elastic brittle material and did not include the localized plastic deformation near the crack tip that occurs in most materials. In 1952, Irwin and Kies[5] and Orowan[6] modified Griffith's theory by introducing a new parameter, γ_p, which represents the localized plastic deformation energy dissipated at the crack tip.

Thus

$$G = 2(\gamma + \gamma_p) \tag{12}$$

From extensive experimental and theoretical approaches to calculating this parameter G, numerous data for different crack geometries and materials have been made available.[7] Unfortunately, the modulus of elasticity of some materials, such as concrete, is difficult to evaluate. Therefore, it is desirable to combine G and E into a single parameter.

2.2 The Stress Intensity Approach

2.2.1 Stress Intensity Factor

Using Westergaard's[2] solution, failure resulting from the stress field which is associated with the crack tip can be

divided into three categories. These categories are generally referred to as:

Mode I tension failure (crack opening)

Mode II inplane shear failure

Mode III antiplane shear failure (twisting)

These failure modes are shown in Figure 2.2

In fracture analysis, Mode I failure is the most important mode, and will be the only one discussed here.

In 1959, by rearranging Westergaard's solution, Irwin[9] obtained a term, K, which depended only on the applied stress and crack length,

$$K_I = \sigma\sqrt{\pi a} \quad \text{(plane stress)} \tag{13}$$

where the subscript I refers to Mode I failure.

The advantage of this parameter K, the stress intensity factor, is that it fully describes the combined effect of the applied stress and the crack length. In the general case of mixed mode fracture, applied stresses due to tension, torsion, point loading, etc., each make their own specific contributions to σ, and the resultant may be calculated simply by adding the individual stress intensities. The effects of specimen shape, body configuration, and boundary conditions on K_I can be incorporated into a geometrical function f(g), so that Eq. 13 becomes

$$K_I = \sigma\sqrt{\pi a}\, f(g) \tag{14}$$

Figure 2.2 The Three Different Modes of Failure (After Knott)[8]

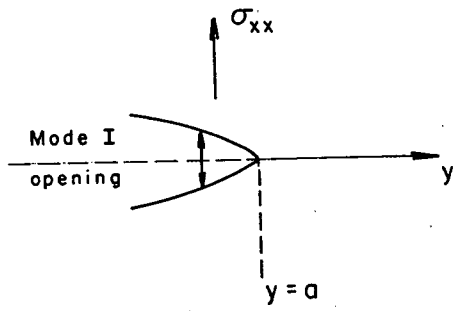

Mode I opening (displacement u in x direction.)

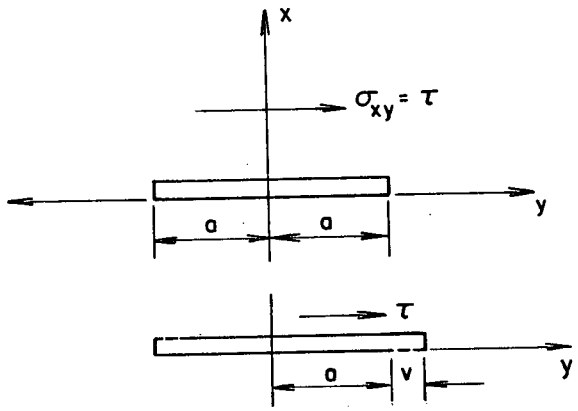

Mode II shear (displacement v in y direction.)

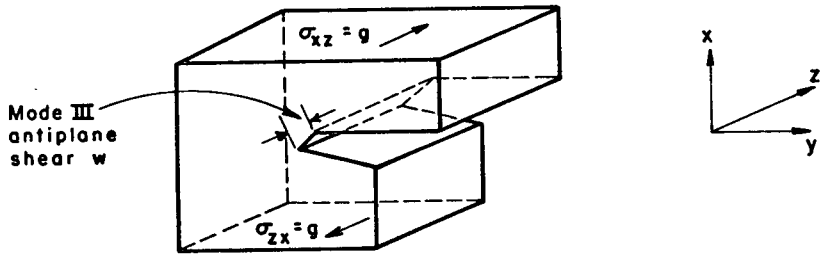

Mode III antiplane shear (displacement w in z direction.)

2.2.2 Effective Crack Length

In metallic materials, plastic deformation of the material near the crack tip creates a plastic zone. The size of this zone, r_y, can be estimated by (10)

$$r_y = \frac{1}{2\pi} \left(\frac{K_I}{\sigma_y}\right)^2 \tag{15}$$

where σ_y = yield strength

The effective crack length, a_e, must include the effect of this zone, hence

$$a_e = (a + r_y) \tag{16}$$

In the case of a plane strain specimen, plastic deformation is more difficult at the center of thick specimens, which are more likely to cleave than to plastically deform. Irwin[11] estimated that the plastic zone for thick specimens is reduced by a factor of 3. Thus, for metallic materials,

$$r_y = \frac{1}{6\pi} \left(\frac{K_I}{\sigma_y}\right)^2 \tag{17}$$

Concrete and other cementitious materials do not deform and develop a "plastic" zone as do metallic materials. However, they do form a large zone of fine cracks around the crack tip. This zone of fine cracks will move with the crack tip as the crack extends.[12] The zone of fine cracks has been called the "pseudo-plastic zone"[13], which can be considered to be equivalent to the plastic zone in metals.

2.3 Relationship Between G and K

Using Westergaard's solution and the energy principle, Irwin[9] showed that the elastic strain energy release rate G and the stress intensity factor K can be related by

$$G = \frac{K^2}{E} \qquad \text{(plane stress)} \tag{18}$$

and

$$G = \frac{K^2}{E}(1 - \nu^2) \qquad \text{(plane strain)} \tag{19}$$

where ν = Poisson's ratio

These relationships enable the strain energy release rate to be expressed directly in terms of values of the stress intensity. Formulation of the relationship involves only the energy principle; no mention of fracture has been made. As the crack moves forward by an amount da, an amount of energy per unit thickness equal to Gda or $(\frac{K}{E})^2 \cdot da$ would be released. Whether this is sufficient to cause catastrophic crack propagation depends on whether the energy released reaches a critical magnitude. This result demonstrates that when the energy release rate is below some critical value, the system may undergo stable crack growth before catastrophic crack propagation occurs. The result also provides a means of understanding stable crack growth. Stable crack growth is important because in a system under load, it may cause a crack which is initially smaller than

the critical size for the applied stress to extend to the critical size, at which point fracture would occur.

2.4 Fracture Mechanics Applied to Fibre Reinforced Concrete

It is now well established that concrete failure is due to progressive internal cracking. Failure is the result of an essentially continuous material changing to an essentially discontinuous one. Richart, Brandtzaeg and Brown[14] first found that the volume of concrete under uniaxial compressive loading initially decreased, as would be expected from elastic theory. However, when the applied load reached about two-thirds of the ultimate load, the volume of the concrete started to increase. At ultimate load, they found that the apparent volume of the concrete specimen was larger than the initial volume of the specimen. From this, they concluded that the bulging and eventual failure of the material resulted from the gradual development of internal tension-induced microcracking throughout the specimen, and this has subsequently been confirmed by many other investigators. Failure takes place when the cracks develop continuous patterns.

In 1963, by introducing aligned steel fibres parallel to the tensile stress in a concrete system, Romualdi and Batson[15] found that the tensile cracking strength of the system increased in proportion to the inverse square root of the wire spacing. They reasoned that as an internal tensile crack propagates in a given material, displacements perpendicular to the plane of the crack develop in the vicinity of the crack tip as a result of the stress singularity in that

region. The presence of a stiffening element in the vicinity of the crack opposes these displacements by means of adhesive coupling between the stiffening element and the matrix. The resulting bond forces are directed toward the crack plane and reduce the magnitude of the extensional stresses in the vicinity of the crack tip. Fracture mechanics principles were used in their work to account for the influence of fibre reinforcement on the crack resisting mechanism. Since then, numerous studies have been carried out to investigate the crack arrest mechanism. Initially, these studies involved only the application of linear-elastic fracture mechanics. However, as an increasing amount of experimental data became available, inconsistencies in the measured fracture parameters such as the critical strain energy release rate, G_{IC}[a] or the critical stress intensity factor (also known as fracture toughness), K_{IC}[a] became apparent. The values of G_{IC} or K_{IC} appeared to be strongly dependent on the specimen geometry and the method of measurement. Recently, a number of investigators have begun applying elastic-plastic fracture mechanics to fibre reinforced concrete. Two of the reasons for extending the linear-elastic criteria into the elastic-plastic region are: (1) concrete itself is not a perfectly brittle material; and (2) fibre reinforcement gives the concrete more apparent ductility. The most common techniques of elastic-plastic fracture mechanics which

---

[a] where subscripts I and C refer to the Mode I failure and the critical value, respectively.

have been applied to fibre reinforced concrete are: (1) the critical crack opening displacement method (COD), (2) the J-integral technique, (3) R-curve techniques and (4) the fictitious crack model. A brief description of these techniques has been given by Mindess[16, 17]. A number of investigations have been carried out using these methods; however, the experimental data indicate some uncertainty in their application as well. While Nishioka, Yamakawa, Hirakawa and Akihama[18] and Brandt[19] claim that COD_c and J_c can be applied to fibre reinforced concrete, Halvorsen[20] and Velazco, Visalvanich and Shah[21] have found that J_c and COD_c depend on the specimen geometry. Although a limited number of experimental results support the R-curve technique, more research is required to clarify its applicability to fibre reinforced concrete.

Chapter 3

MEASUREMENT OF FRACTURE PARAMETERS AND STABLE CRACK GROWTH

3.1 Test Specimens

A number of specimen geometries have been developed to measure fracture parameters and crack propagation. The most common are

1. Edge cracked tensile specimen
2. Centre cracked tensile specimen
3. Double cantilever beam specimen
4. Double torsion specimen

Edge cracked tensile specimens and centre cracked tensile specimens such as the compact tension speciman and the notched beam specimen have been adopted in ASTM Standard E561-80 for fracture testing of metallic materials. However, the double torsion and double cantilever beam specimens are more frequently used on ceramic materials to measure slow crack growth and fracture toughness. One of the reasons for their popularity is that with these specimens, the fracture toughness is independent of the crack length over a substantial range of crack growth. These specimens also allow several determinations of fracture toughness on a single specimen.

Both double cantilever beam and double torsion specimens have the same initial geometry. Basically they are rectangular plates with a centre groove running the full length of the plate. However, in the double torsion technique, torsional loading is used to propagate the crack, rather than the tensile

loading of the double cantilever beam technique. In the double cantilever beam technique, crack velocity studies are usually performed using the fixed loading technique. The crack velocity is calculated by measuring the length of the crack increment and the time required for such an increment. The position of the crack is monitored optically. An equivalent method can also be used in crack velocity studies with the double torsion technique. Slow crack growth data are also obtained under a constant load, and the crack growth rate can be monitored optically. Under these conditions, both techniques should be equivalent. As an alternative, using a constant displacement or a constant displacement rate to propagate the crack, Evans[22] showed that by using compliance methods, the crack growth rate can be calculated directly from the applied load, P, or the load relaxation rate dp/dt. Both the crack velocity and the stress intensity can be determined from the load. This method therefore provides a simple way of monitoring crack growth when direct visual observation of the crack tip is impossible.

3.2 Double Torsion Technique

By considering the double torsion specimen shown in Fig 3.1 as two rectangular elastic sections, Williams and Evans[23] showed that the stress intensity is a function only of the specimen dimensions, the applied load and Poisson's ratio. The stress intensity can be expressed as

Figure 3.1 The Double Torsion Specimen

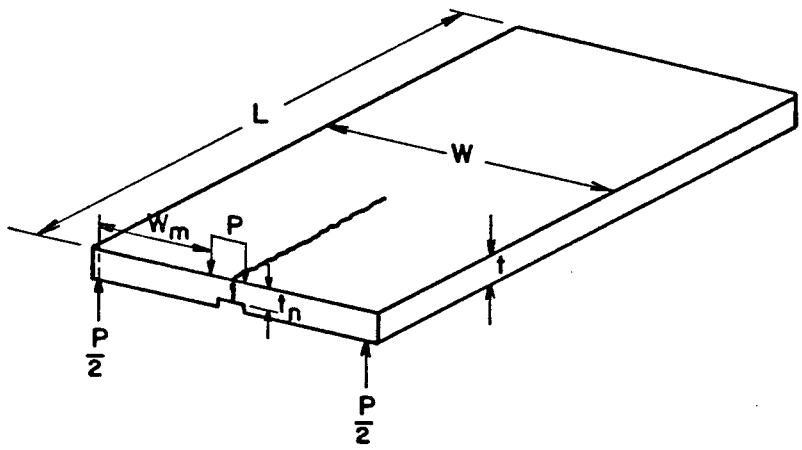

$$K_I = P\omega_m \left[\frac{3\,(1+\nu)}{Wt^3 t_n}\right]^{\frac{1}{2}} \qquad (20)$$

where K_I = stress intensity factor

P = applied load

ω_m = moment arm

ν = Poisson's ratio

W = width of the specimen

t = thickness of the specimen

t_n = plate thickness in the plane of the crack

They confirmed that the compliance C and the crack length "a" are linearly related. The system compliance can be expressed as

$$C = \frac{y}{P} \doteq (Ba + c) \qquad (21)$$

where y = deflection

B = slope of the V-K_I curve

c = the intercept of the V-K_I curve

With the compliance expression, Williams and Evans[23] also showed that for constant displacement or constant displacement rate, the crack growth rate can be related to the instantaneous load and the corresponding load relaxation rate dp/dt as

$$V = \frac{y}{BP^2}\left(\frac{dp}{dt}\right) = \frac{-(P_{i,f})(a_{i,f})}{P^2}\left(\frac{dp}{dt}\right) \qquad (22)$$

where subscripts i and f represent the initial and final states, respectively.

Hence, the velocity of the crack can be measured over a range of K_I values from a single experiment.

Chapter 4

EXPERIMENTAL PROCEDURE

4.1 Materials

CSA Type 10 (ASTM Type 1) normal Portland cement was used to prepare the concrete. The fine aggregate was commercially available concrete sand, and the coarse aggregate was 3/8"(9.5 mm) pea gravel. All aggregate were stored at ambient laboratory moisture conditions. To improve the workability of the mixes, two types of admixtures were used, an air entraining agent[a] and a water reducing agent[b].

Three types of fibres were used. These were alkali-resistant fibreglass[c], straight steel fibres[d] and deformed steel fibres[e]. Two types of fibreglass were used — 102 filaments per fibre bundle and 204 filaments per fibre bundle. They were chopped strand in 1.0 in.(25.4 mm) lengths. The straight steel fibres consisted of 0.50 in.(12.7 mm) and 1.0 in.(25.4 mm) long fibres with cross-sectional dimensions 0.01 x 0.022 in.(0.254 x 0.559 mm). The deformed steel fibres were 0.022 in.(0.559 mm) in diameter with hooked ends, as shown in Table 4.1.

---

[a] MBVR, supplied by Master Builders Co.
[b] Liquid pozzolith, type 300N, supplied by Master Builder Co.
[c] Supplied by Owens-Corning
[d] Supplied by Stelco, Hamilton, Ontario
[e] Supplied by Bekaert Steel Wire Corp.

TABLE 4.1 MIX DESIGNS

Mix Series	Fibre Volume % by Volume	Weight (lb)					Dosage (ml.)	
		Cement	Water	Sand	3/8" Gravel	Fibre	Pozzolith	AEA
Glass fibre (GF)	0	85	42.5	173	53	0	100	12
	0.25	"	"	173	53	1.14	"	"
	0.5	"	"	171.5	56.7	2.27	"	"
	0.75	"	"	170.7	56.5	3.41	"	"
	1.0	"	"	169.8	56.2	4.54	"	"
	1.25	"	"	169.0	55.9	5.7	"	"
	1.5	"	"	168.0	55.6	6.8	"	"
	2.0	"	"	166.4	55	9.1	"	"
Straight steel fibre (SSF)	0	67.5	24	148	148	0	58	23
	0.25	"	25	146.5	146.5	3.3	"	"
	0.5	"	26.5	144.5	144.5	6.7	"	"
	0.75	"	27	142.5	142.5	10	"	"
	1.0	"	28	141	141	13.5	"	"
	1.25	"	28.5	140	140	17	"	"
	1.5	"	29	139	139	20	"	"
	2.0	"	30	136	136	27	"	"
Deformed Steel Fibre (BSF) 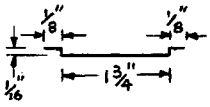	0	67.5	33.8	148	148	0	58	23
	0.25	"	"	147.4	147.4	3.27	"	"
	0.5	"	"	146.8	146.8	6.53	"	"
	0.75	"	"	146.3	146.3	9.8	"	"
	1.0	"	"	145.7	145.7	13.1	"	"
	1.25	"	"	145.1	145.1	16.3	"	"
	1.5	"	"	144.5	144.5	19.6	"	"
	2.0	"	"	143.3	143.3	26.1	"	"

4.2 Design of Specimen and Mold

The dimensions of the double torsion specimens were proportioned from smaller specimens previously used by Nadeau, Mindess and Hay[24]. All specimens were cast in steel molds, each 48 x 16 x 2.0 inches (1219 x 406.4 x 50.8 mm). Each mold contained a 48 in. (1219 mm) long bar with a tapered cross section, 1.0 in. (25.4 mm) in depth x 0.50 in. (12.7 mm) at base x 0.25 in. (6.35 mm) at the top for molding the precast groove, as shown in Figure 4.1. A coating of oil was applied to the mold before casting so that the concrete would not adhere to the mold. Specimens were removed from the mold by simply disassembling the mold.

4.2.1 Casting of Specimens

All mixes were prepared in a pan-type mixer, with the ingredients weighed on a balance accurate to 1.0 lb. The air entraining agent was diluted with the mixing water while the workability agent was first poured into the fine aggregate and allowed to be absorbed. This procedure was intended to prevent direct chemical reaction between the workability aid and the air entraining agent. The pan was first dampened, and the coarse and fine aggregates plus two thirds of the mixing water were placed in the mixer and mixed thoroughly. The cement was then added and mixed in until it was uniformly distributed throughout the batch. The remaining water was then added. Fibre reinforcement was added by shaking the

Figure 4.1 Casting Mold

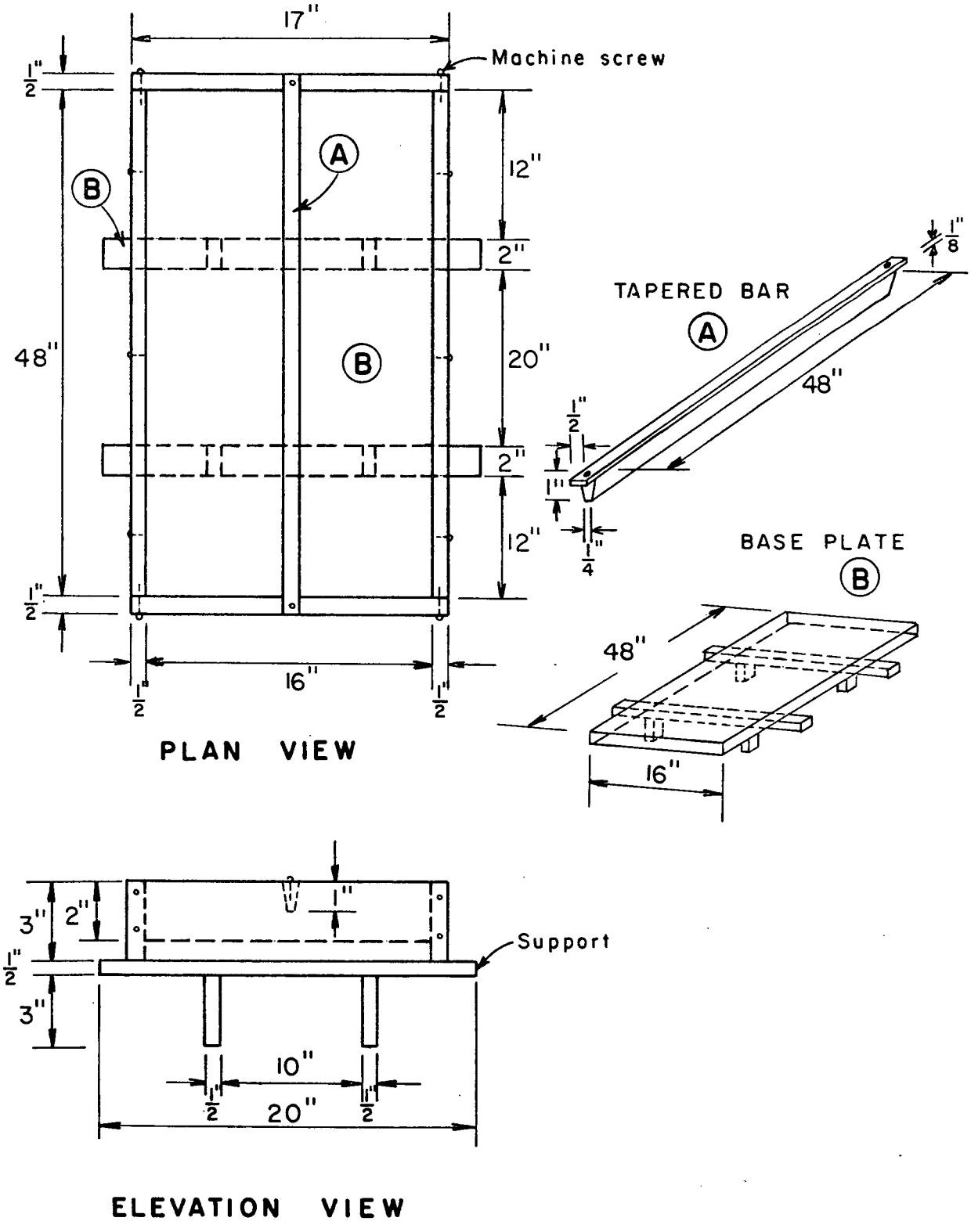

fibres through a sieve to prevent "balling", and the concrete was mixed for a further five minutes. After mixing, the concrete was placed into the oiled mold with a shovel and compacted using an immersion vibrator. Finally, the specimens were finished with a trowel and covered with plastic to prevent drying. Specimens were removed from the mold after 24 hours and kept in a moist room until testing. The age of the specimens was about 3 years at the time of testing.

4.2.2 Preparation of Specimen before testing

A day before the testing of any specimen, a coating of plaster of Paris was applied on the non-grooved side of the specimen. This procedure was intended to aid in observing crack growth on the tension side of the specimen during testing. Just prior to testing, the specimen was removed from the moist room and a coat of a commercial curing agent was applied on the specimen to prevent loss of moisture due to evaporation during testing. An initial crack, 4.0 in. (101.6mm) long, was cut in the centre of one end of the specimen along the groove, using a diamond saw. The crack was cut in such a way that the leading edge was on the grooved surface. A loading jig, with four clamps and four loading points, was fixed in the testing machine. Details of this jig are shown in Figure 4.2. The prepared specimen was secured to the loading jig with the precracked edge over the load points and the tension side up (Figure 4.3). The edges of the specimens were aligned parallel with the sides of the loading jig. The distances between the edges of the

Figure 4.2 Loading Jig

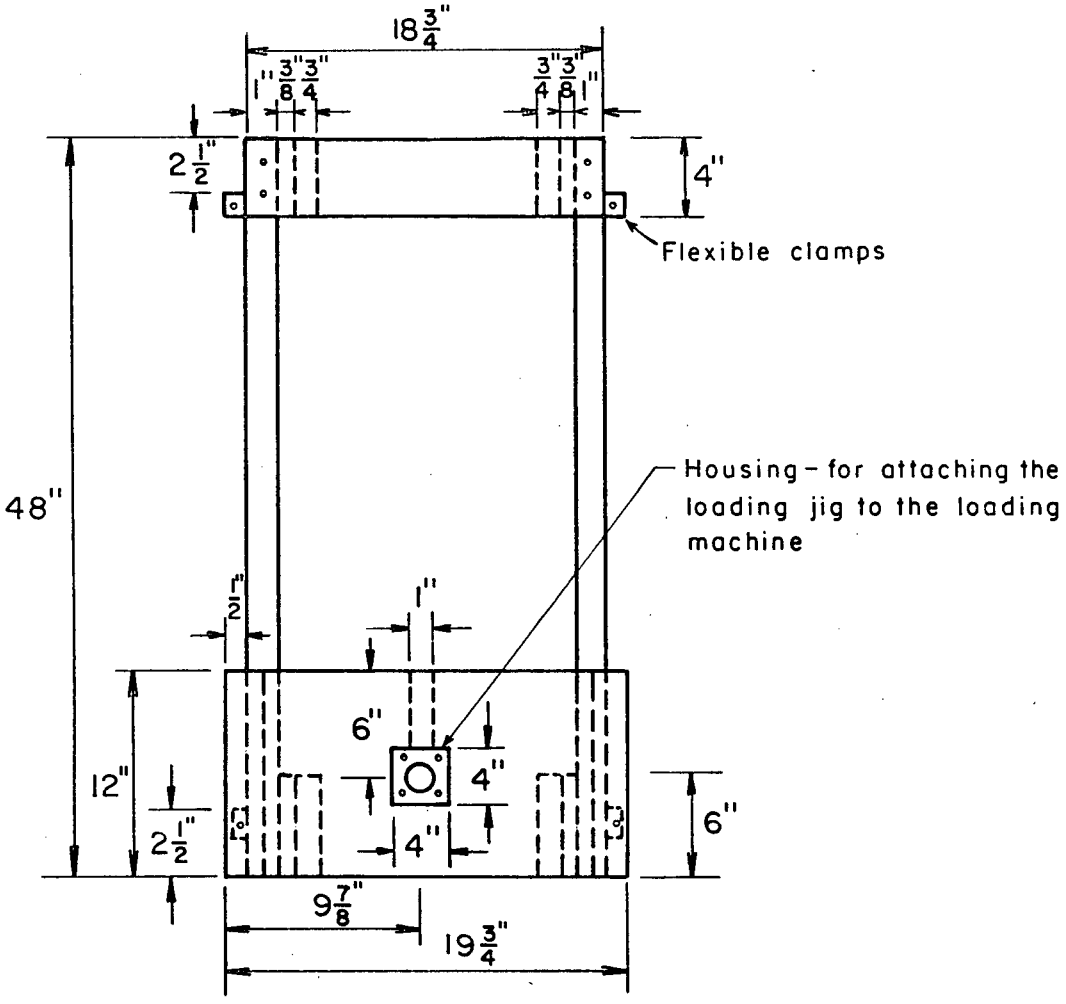

PLAN VIEW

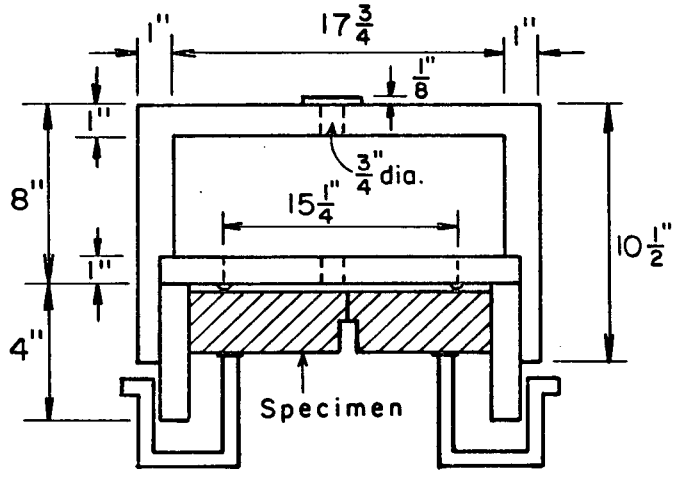

ELEVATION VIEW

Figure 4.3 Test Setup

specimen and the loading points were kept equal. An external load cell of 2000 lbf capacity, with two ball-bearings as loading points, was placed under the precracked side of the specimen (Figure 4.4). The loading configuration was so arranged that when the cross-head of the testing machine[a] descended the load cell acted as a rigid support. The two ball-bearings, one on either side of the crack, thus applied the required force to the specimen. Figures 4.5 and 4.6 show the testing setup.

There are two main advantages of this loading configuration. First, the ball-bearings were placed under the specimen instead of hanging above it. This eliminated the necessity of a fixture to hold the ball-bearings in their housing. Second, the tension surface was located on the top of the specimen. This provided the possibility of observing crack propagation with ease. A strip chart recorder, calibrated with the external load cell, was connected to the load cell to record the applied load and elapsed time. The chart speed was 2.0 in/min (50.8 mm/min).

4.3 Test Program

Two types of tests were performed.

4.3.1 Compliance Test

The material compliance of the specimen was obtained

---

[a] Tinius Olsen, 200000 lb capacity mechanical loading machine

Figure 4.4 External Load Cell

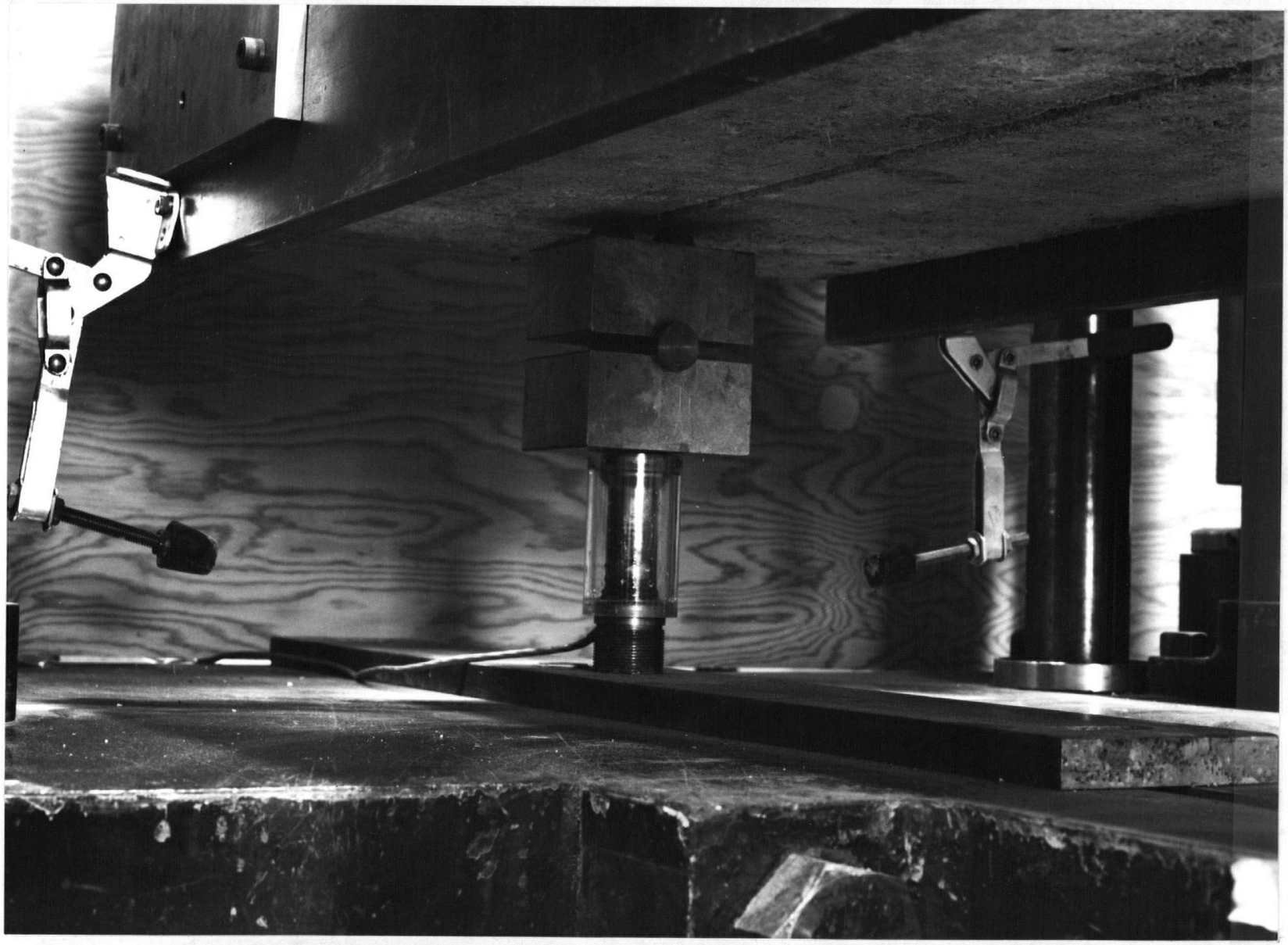

Figure 4.5 Front View Of The Test Setup

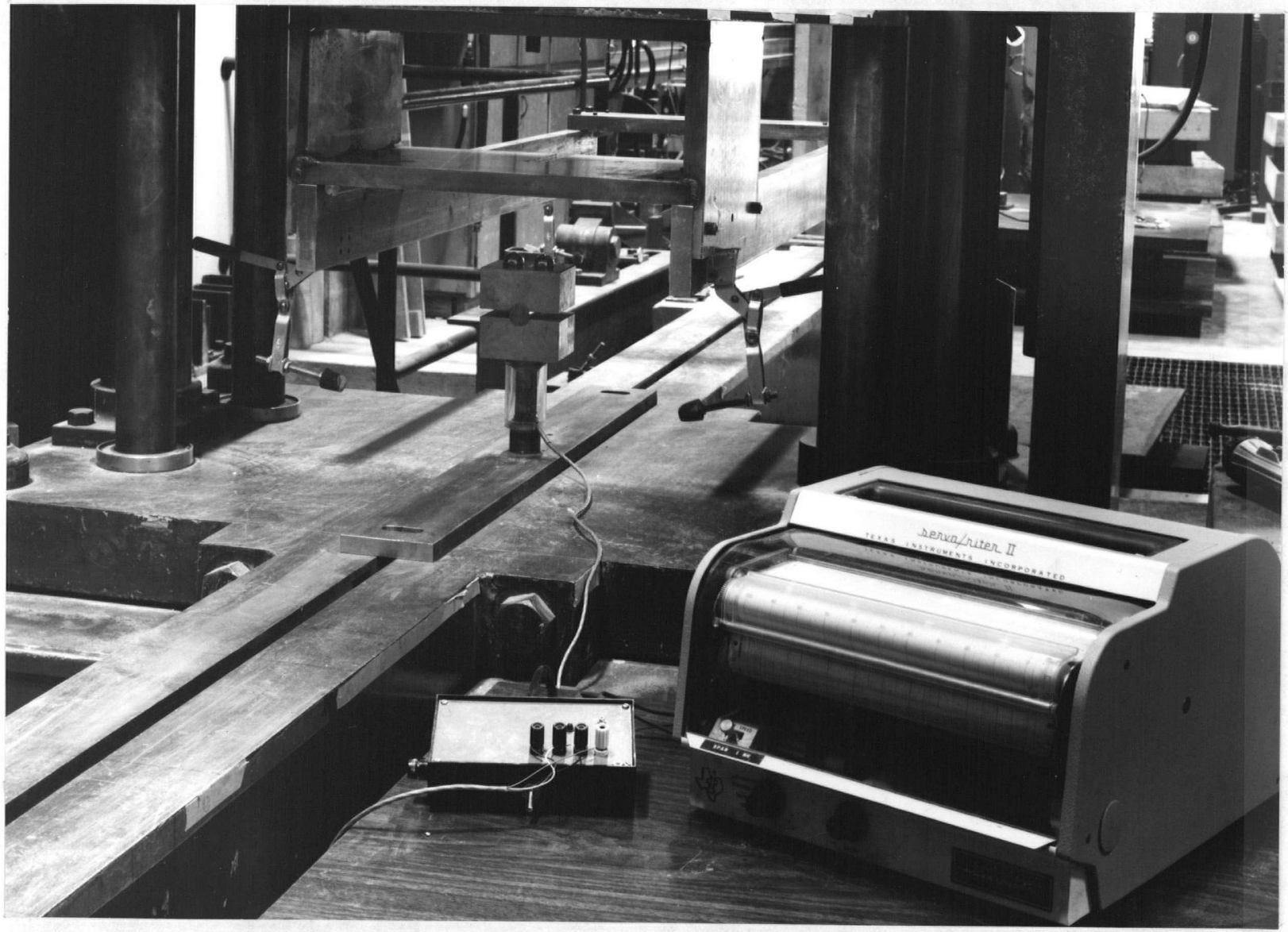

Figure 4.6 Side View of the Testing Setup with a Specimen Inplace

by measuring the applied load and the corresponding deflection as follows. The specimen was first prepared and set on the loading jig as described in Section 4.2.2. Two dial gauges, one placed next to the load cell and one placed at the outer edge of the specimen, were used to measure deflections. The load was applied to the specimen in 200 lb increments. Readings of the dial gauges and the corresponding applied load were recorded. The deflection of the plate was obtained by subtracting the reading of the dial gauge placed on the outer edge of the specimen from the reading of the one near the load cell. After a set of compliance measurements was made, the specimen was removed from the loading apparatus. A longer crack was cut using a portable ceramic electric power saw. These procedures were then repeated with different crack lengths.

4.3.2 Double Torsion Test

The load relaxation method[25,26] was used on double torsion specimens to determine the relationship between crack velocity and stress intensity. Readings of applied load and corresponding elapsed time were recorded. During testing, the cross-head of the testing machine was first lowered so that the specimen was just touching the two loading points of the load cell. Once contact was made, the two clamps on the loading side were released. Load was applied by lowering the cross-head with a constant speed of 0.0373 in/min (0.947

mm/min). Load relaxations were performed at every two hundred pound increment, by simply stopping the cross-head movement. When the crack started to propagate, this usually resulted in the load-elapsed time curve deviating from linearity, and the cross-head was stopped immediately. The nonlinearity of the curve signalled a change of compliance in the specimen. With the cross-head fixed, the load continued to fall slowly as the crack grew at a decreasing rate. Each point on the resulting load-time curve corresponded to a different crack velocity and stress intensity. Thus, a $V-K_I$ plot could be obtained from a single load-relaxation curve. Background relaxation was measured as the load-relaxation curve for the last relaxation obtained for the specimen before the load dropped, and this was subtracted from the apparent load relaxation curve. The loading procedure was resumed after measuring the first crack propagation and stopped when the crack finally propagated down the plate. Figures 4.7 to 4.9 show the crack appearance at various stages.

The new crack tip was located with the aid of a 10x magnifying glass and marked on the specimen. However, this apparent crack tip was found to be misleading, due to the nature of the observed crack. Before a visible crack could be observed on the surface, microcracks visible only using very high magnification have probably already propagated

Figure 4.7 Initial Stage of Crack Propagation

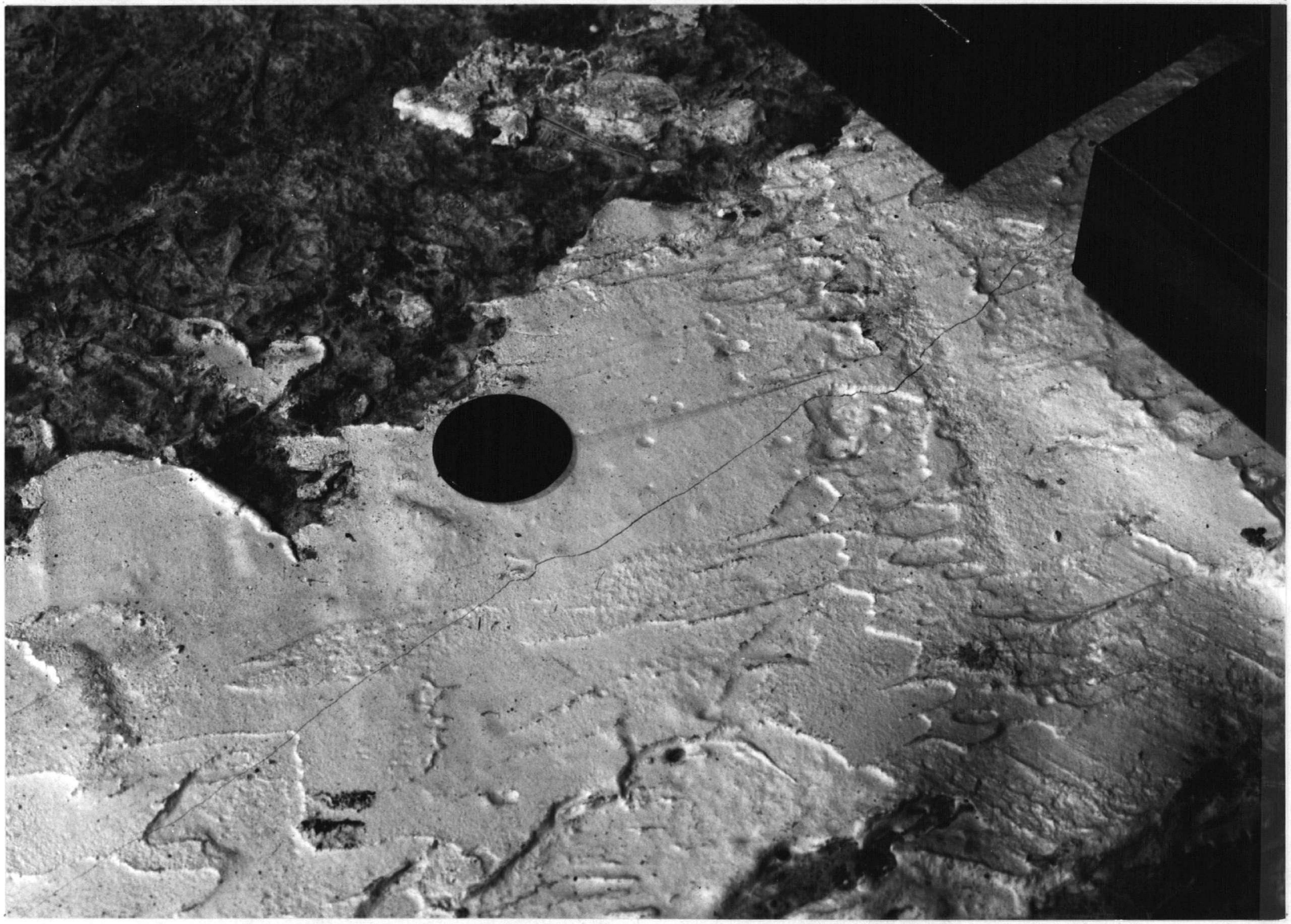

Figure 4.8 Specimen Just Before Failure

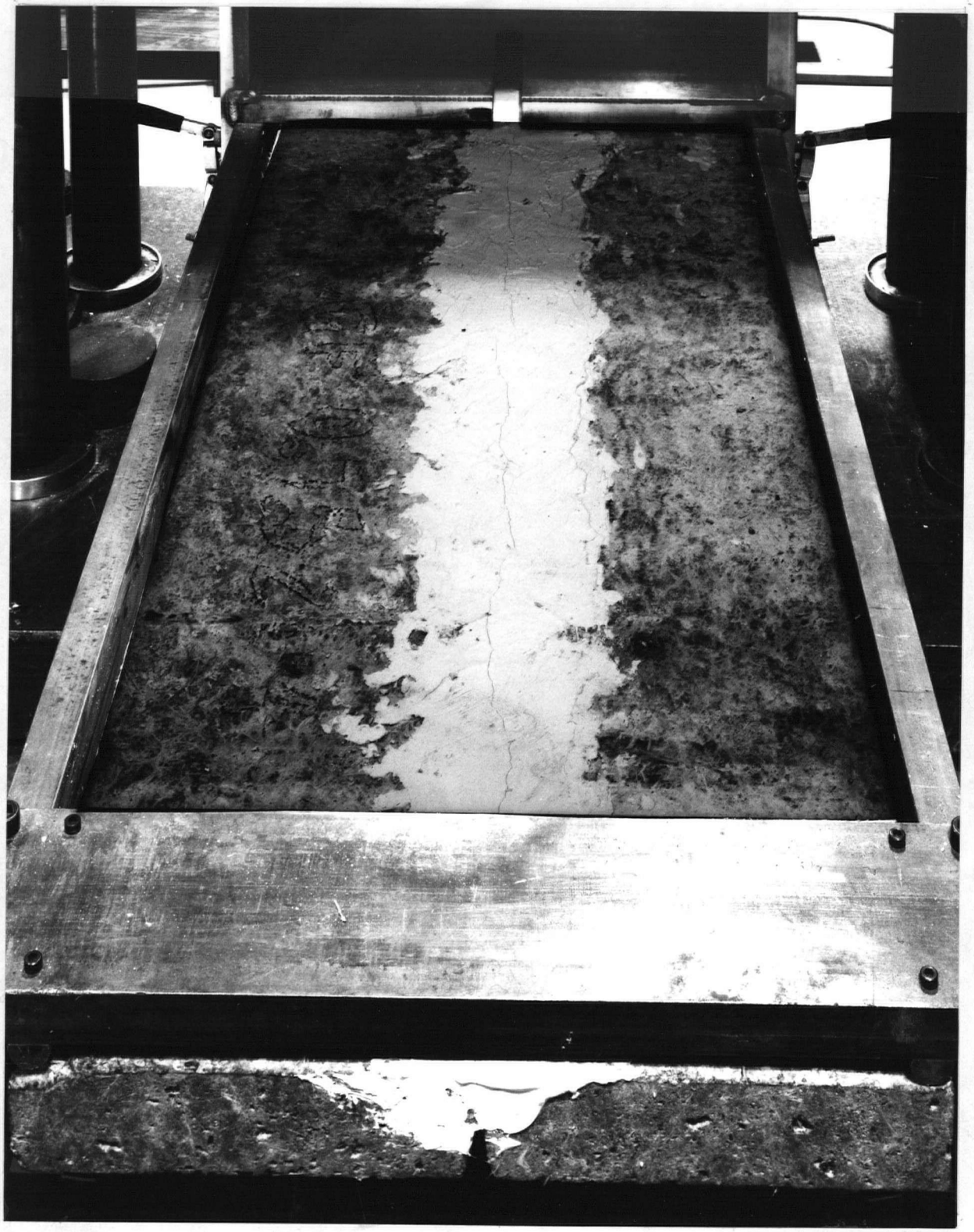

Figure 4.9 Specimen After Failure

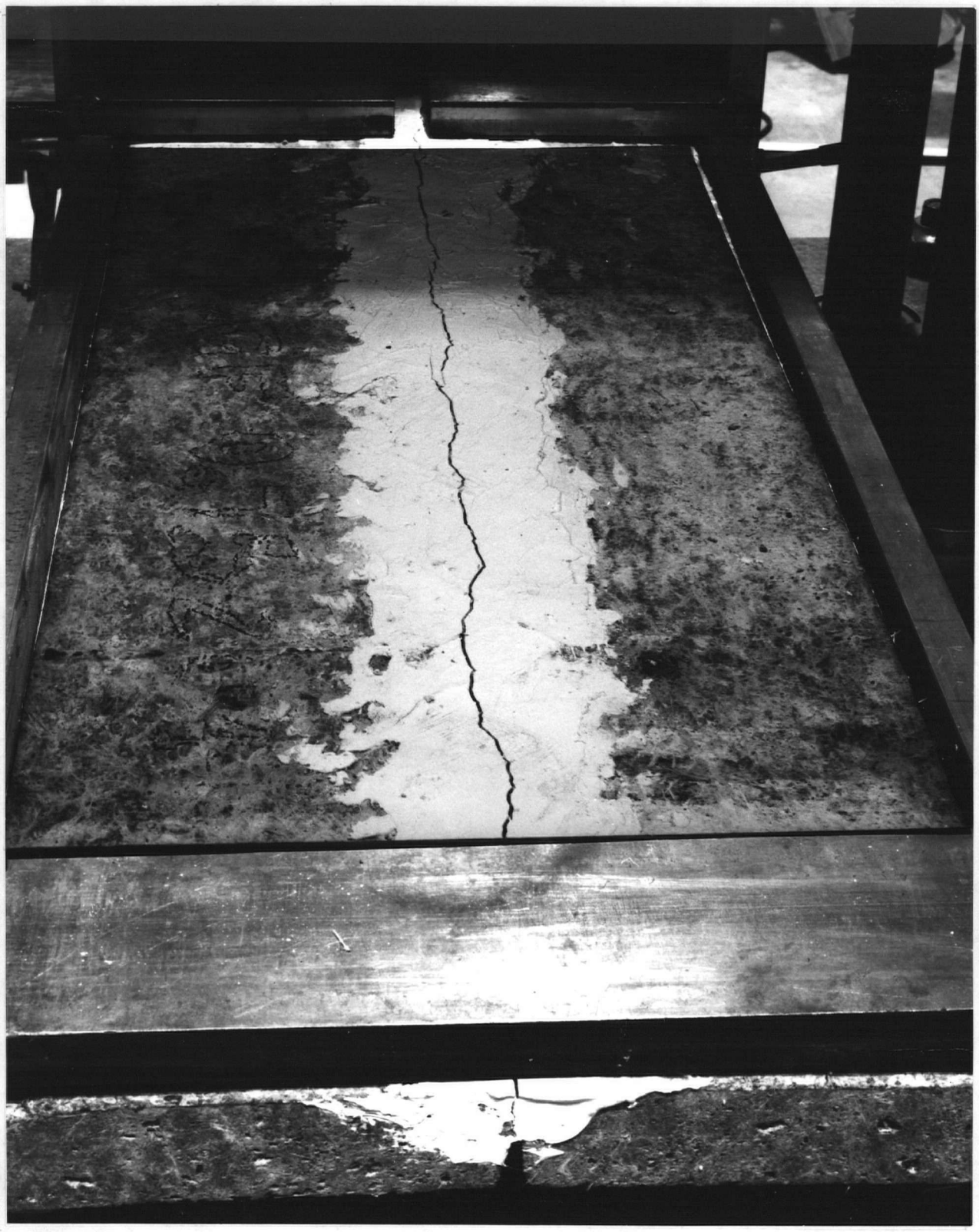

beyond the visible crack. Therefore, the measured value would tend to underestimate the true crack length. Thus this procedure was discontinued. Other efforts were made to measure the true crack length by using a penetrating dye. Unfortunately, the results were less than satisfactory due to the roughness of the crack surface. The penetrating dye tended to disperse and became blurred; thus a definite crack front could not be obtained.

Chapter 5

EXPERIMENTAL RESULTS

5.1 Introduction

The main object of this research was to investigate the effect of fibre reinforcement on crack growth in concrete. Crack propagation data were obtained using the load relaxation method on a double torsion specimen as described above. In all, thirty-one specimens were tested and the results are shown in Tables B1 to B31 (Appendix B).

In the glass and deformed steel fibre specimens, the fibre content was the only variable. The w/c ratio for these specimens was 0.5. Both the fibre content and the w/c ratio were varied in the straight steel fibre series (see Table 4.1).

5.2 Cement Paste Specimens

To obtain some indication of the validity of the test results, two specimens of cement paste (w/c = 0.4) were made and tested. The results were then compared with available data from the literature to see whether the values obtained were of the right order of magnitude. The age of the specimens at testing was 90 days. The test results are tabulated in tables 5.1 and 5.2.

The data in Tables 5.1 and 5.2, and Tables B1 to B31 can be described as follows:

TABLE 5.1

Load Relaxation Data for Cement Paste No. 1

Fiber volume: 0

Load at failure: 600 lb.

Load after failure: 0

Apparent Relaxation (a)					Corresponding Background Relaxation (b)				True Relaxation	Velocity	Stress Intensity
load lb p	load lb dp	paper (in) dm	time (sec) dt	slope $(\frac{dp}{dt})_b$	load lb dp	paper (in) dm	time (sec) dt	slope $(\frac{dp}{dt})_a$	$(\frac{dp}{dt})_a - (\frac{dp}{dt})_b$	$V \times 10^{-2}$ in/sec	K $\frac{1}{2}$ ksi-in
300	280	0.6815	20.6	13.57	75	2	60	1.25	12.32	11.4	0.364
280	200	1.038	58.125	3.44	50	2	60	0.833	2.607	1.8	0.34
265	62	4.5	135	0.459	48	6.75	202.5	0.237	0.222	0.18	0.325
260	10	2.5	75	0.133	10	6.75	202.5	0.049	0.084	0.067	0.316

Initial Load 330 lb.

TABLE 5.2

Load Relaxation Data for Cement Paste No. 2

Fiber volume: 0

Load at failure: 540 lb.

Load after failure: 0

Apparent Relaxation (a)					Corresponding Background Relaxation (b)				True Relaxation	Velocity	Stress Intensity
load lb p	load lb dp	paper (in) dm	time (sec) dt	slope $(\frac{dp}{dt})$	load lb dp	paper (in) dm	time (sec) dt	slope $(\frac{dp}{dt})$	$(\frac{dp}{dt})_a - (\frac{dp}{dt})_b$	$V \times 10^{-2}$ in/sec	K $\frac{1}{2}$ ksi-in
280	150	0.5	15	10	120	4.69	140	0.853	9.147	16.7	0.332
260	160	1.44	43.13	3.71	40	2.56	76.88	0.52	3.19	6.1	0.313
245	64	2.16	64.69	0.989	18	4	120	0.15	0.839	1.8	0.294
240	40	4.5	135	0.296	8	9	270	0.029	0.267	0.34	0.291
235	8	7.5	225	0.036	2	6	180	0.011	0.025	0.015	0.285

Initial Load 318 lb.

Column 1 applied load

Columns 2-5 describe the slope of the relaxation curve at the applied load

In describing the slope of the relaxation curve at the applied load, a horizontal line was drawn which intercepted the apparent relaxation curve at the applied load (Figure 5.1). The slope of the curve was obtained by constructing a tangent to the curve at the intercepted point.

Column 2 difference in the vertical axis (y-axis) i.e. difference in load dp

Column 3 difference in the horizontal axis (x-axis) i.e. difference in chart length dm

Column 4 difference in time, dt where

$$dt = \frac{dm}{\text{chart speed}} = 30\ dm$$

Column 5 slope of the apparent relaxation curve at the applied load.

The corresponding background relaxation was obtained by reproducing the background relaxation curve of the specimen below the apparent relaxation curve (see Figure 5.1) with the initial load drop of the curves at the same x-value. A vertical line was drawn through the intercepted point of the applied load on the apparent relaxation curve which cut a point on the background relaxation curve. A tangential line was drawn to the background relaxation curve at this point. The slope of this line was the corresponding background

Figure 5.1 Load Relaxation Curves

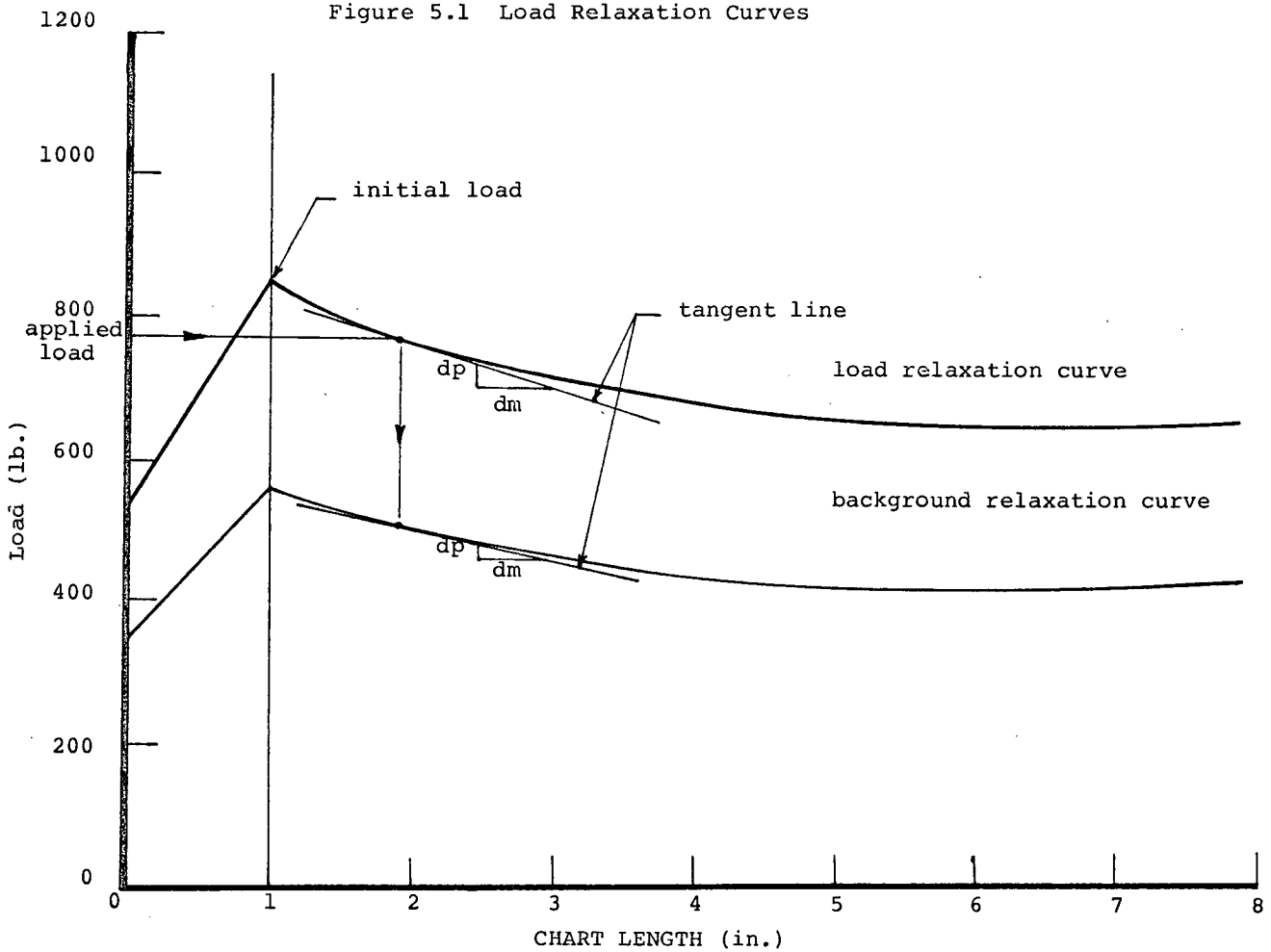

relaxation. The slope of the background curve is described in Columns 6-9, which are similar to Columns 2-5.

Column 10	true relaxation = apparent relaxation - corresponding background relaxation
Column 11	crack velocity at the applied load
Column 12	stress intensity at the applied load

Typical load relaxation curves are shown in Figure 5.2. These curves can divided into two parts; i) positive slope region, and ii) negative slope region. In the first part, as the load increases, the slope of the curve will remain constant as long as the compliance of the specimen remains constant. When the crack starts to propagate, the slope of the curve first decreases drastically, and then decreases at a much more gradual rate. This suggests that most of the crack propagation occurs during the early part of the relaxation curve. The background relaxation curve is obtained shortly before the crack starts to propagate. This background relaxation is due to the relaxation of the loading machine, and perhaps also due to creep in the specimens. The background relaxation curve is subtracted from the load relaxation curve in order to get the true load relaxation of the specimen. Typically, the curves are sufficiently different only for the first 90 seconds. A sample calculation of the crack velocity is shown in Appendix A.

Figure 5.2 Typical Load Relaxation Curve

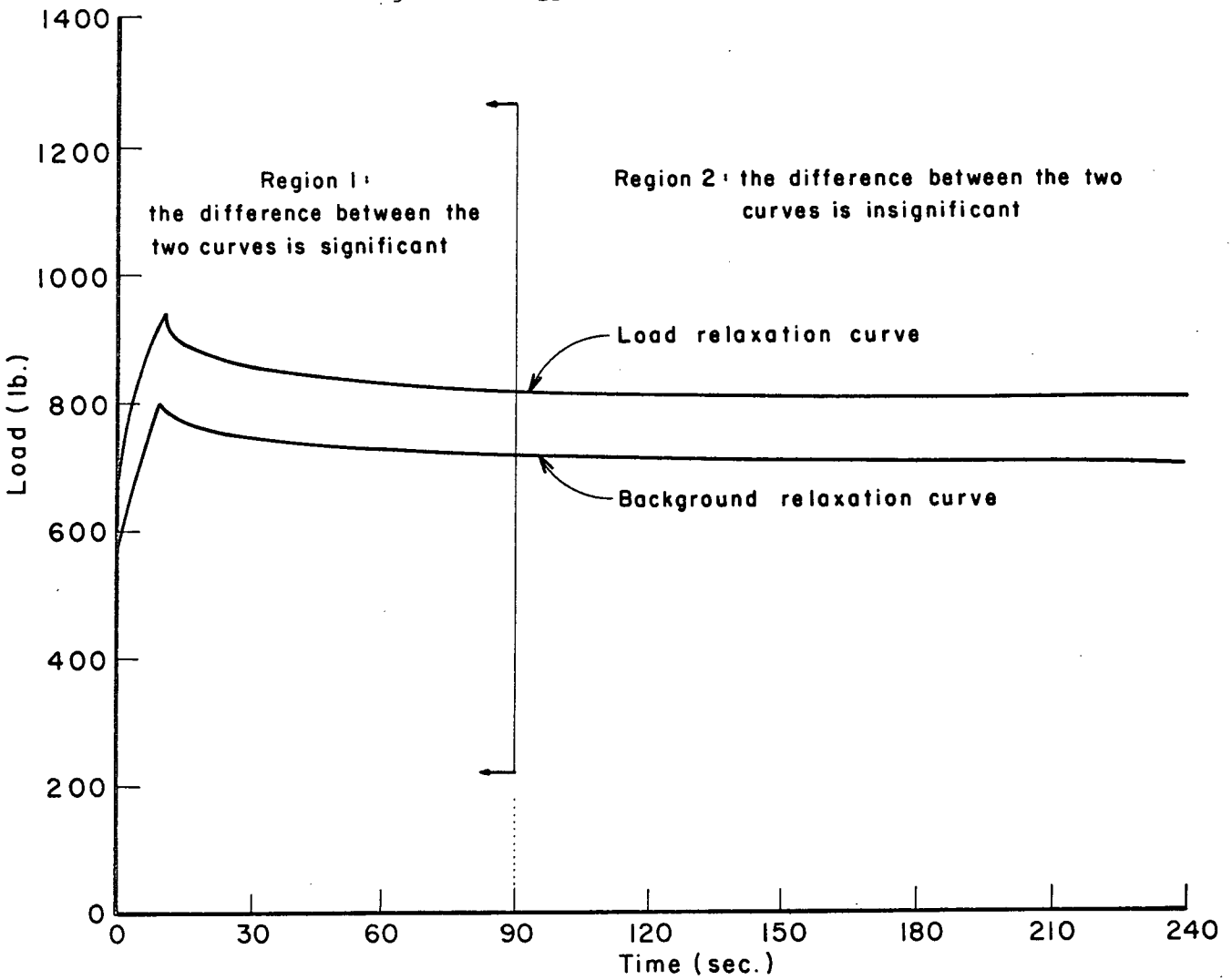

A $V\text{-}K_I$ plot for the results of the two cement paste specimens, and the average $V\text{-}K_I$ plot, are shown in Figure 5.3. The slope of the average $V\text{-}K_I$ curves is 37.6. With the same geometry but a smaller specimen (9.0 x 3.0 x 0.5 in. or 228 x 76.2 x 12.7 mm), Nadeau, Mindess and Hay[24] found that the slope of the $V\text{-}K_I$ curve was approximately 35. The value of the fracture toughness of the control specimen was 0.69 ksi-in$^{\frac{1}{2}}$ (0.75 MN$^{-3/2}$) compared to the value of 0.293 ksi-in$^{\frac{1}{2}}$ (0.32 MN$^{-3/2}$) obtained by Nadeau, Mindess and Hay[24]. Wecharatana and Shah[27], using 32 x 6.0 x 1.5 in. (812 x 152 x 38.1 mm) double torsion specimens, found that the fracture toughness was 1.2 ksi-in$^{\frac{1}{2}}$ (1.31 MN$^{-3/2}$). In both cases (24,27), the w/c ratio was 0.5. The value obtained seems therefore to be within the range of values reported in the literature.

5.3 Fracture Toughness

One of the questions about fibre reinforcement is its effectiveness in increasing the fracture toughness of concrete. The fracture toughness, K_{IC}, of the specimens is tabulated in Table 5.3, and is plotted against the fibre volume in Figures 5.4 to 5.8. (A sample calculation of the fracture toughness is shown in Appendix A). In general, the fracture toughness increases with fibre volume up to about 1.25%. The stress intensity factor, K_I, at the first crack (the first observed visible crack) is tabulated in Table 5.3. The value of this K_I is approximately equal to 70% of the corresponding K_{IC}.

Figure 5.3 V-K_I Plot For The Average Of The Two Cement Specimens

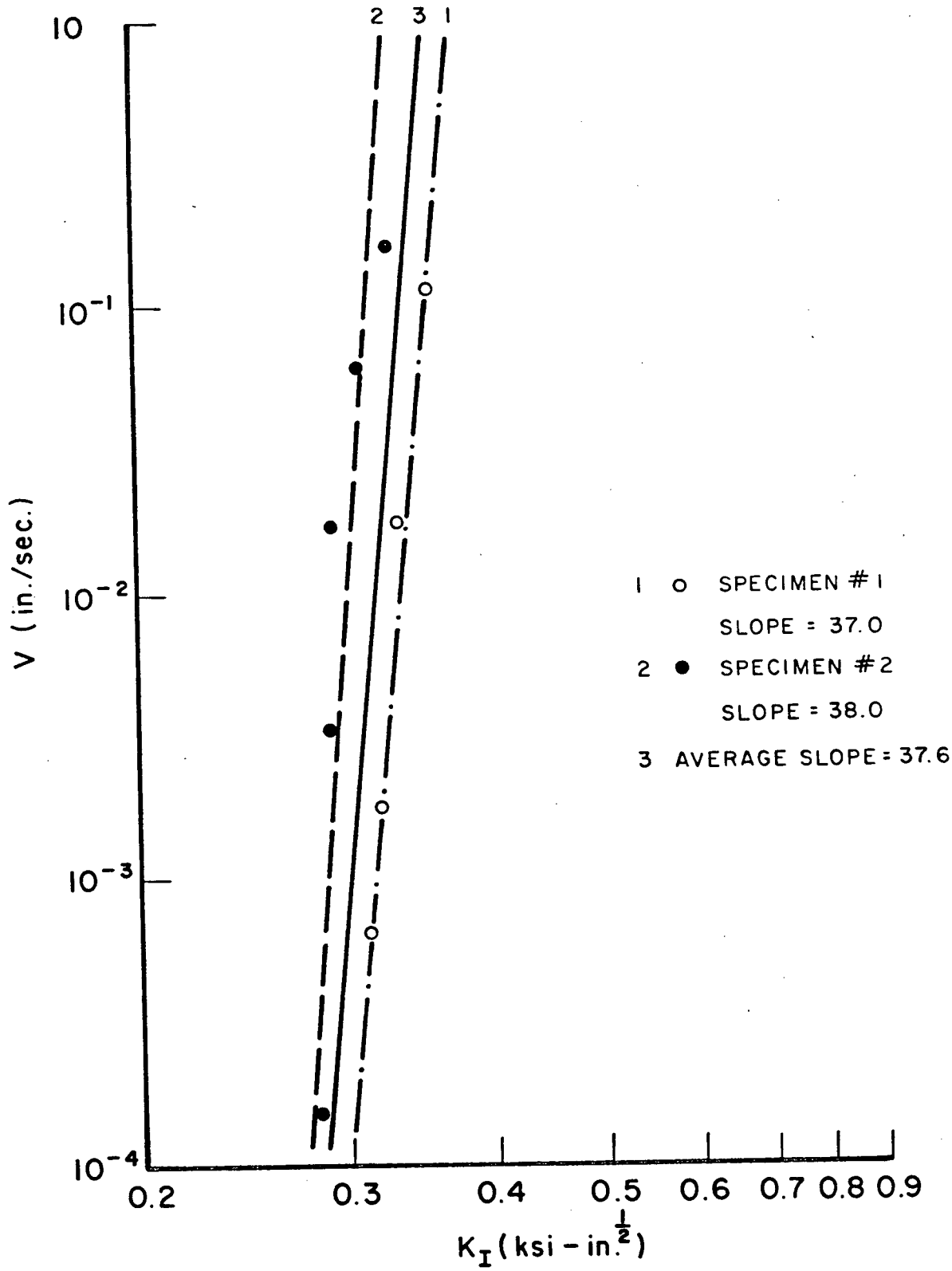

TABLE 5.3 FRACTURE TOUGHNESS AND RESIDUAL STRENGTH OF SPECIMEN

SERIES	FIBRE CONTENT %	K_{IC} (KSI-IN$^{\frac{1}{2}}$) CRITICAL	K_I (KSI-IN$^{\frac{1}{2}}$) AT FIRST CRACK	RESIDUAL STRENGTH (lb)
GF102	0	1.39	1.11	100
	0.25	1.25	1.15	120
	0.50	1.44	0.96	80
	0.75	1.62	1.21	400
	1.0	1.94	1.21	1050
	1.25	2.05	1.32	580
	1.50	2.42	1.94	1420
	2.0	1.81	1.69	1040
GF204	0.25	1.39	1.21	240
	0.5	1.25	1.21	240
	0.75	1.69	1.45	244
	1.25	2.32	2.05	800
	1.5	1.99	0.97	960
	2.0	1.30	0.97	780
½"SSF	0	2.36	1.93	240
	0.25	0.81	0.73	300
	0.5	1.79	0.97	740
	0.75	1.86	1.21	680
	1.25	0.99	0.91	700
	1.5	2.05	1.69	960
	2.0	2.40	1.93	1290
1"SSF	0.25	0.87	1.12	580
	0.5	1.88	1.58	540
	1.0	2.42	1.45	1100
	1.25	2.29	1.38	1180
	1.5	1.25	0.97	660
BSF	0	1.41	1.33	120
	0.25	1.69	1.44	600
	0.5	1.42	1.21	820
	1.25	2.00	1.69	1300
	1.5	2.04	1.69	1390
	2.0	2.36	1.45	1680
Cement 1	0	0.728	1.485	0
Cement 2	0	0.655	0.448	0

Figure 5.4 Relationships Between Fracture Toughness, Weight Density, Residual Strength and Fibre Volume for GF 102 Series

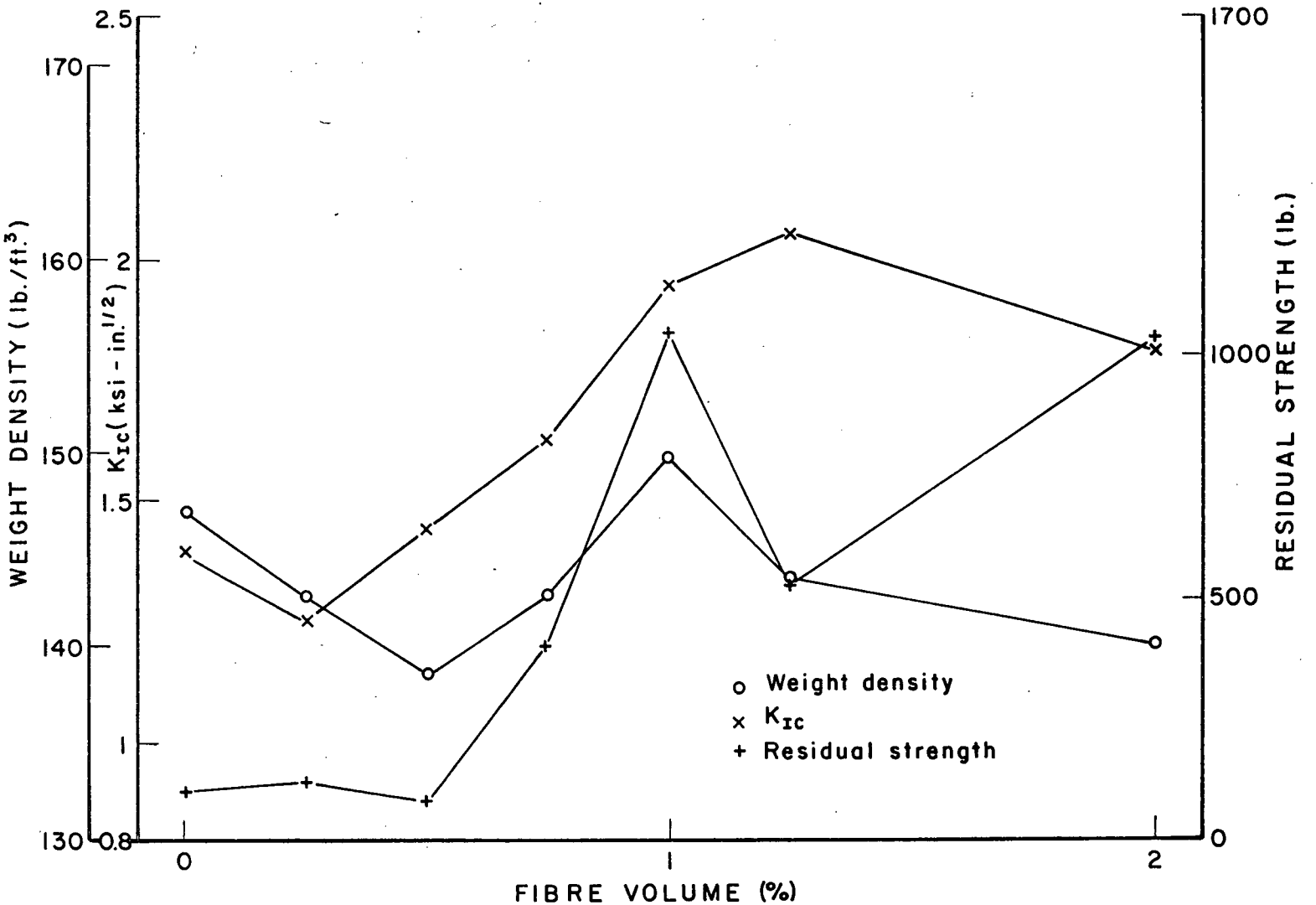

Figure 5.5 Relationships Between Fracture Toughness, Weight Density, Residual Strength and Fibre Volume for GF 204 Series

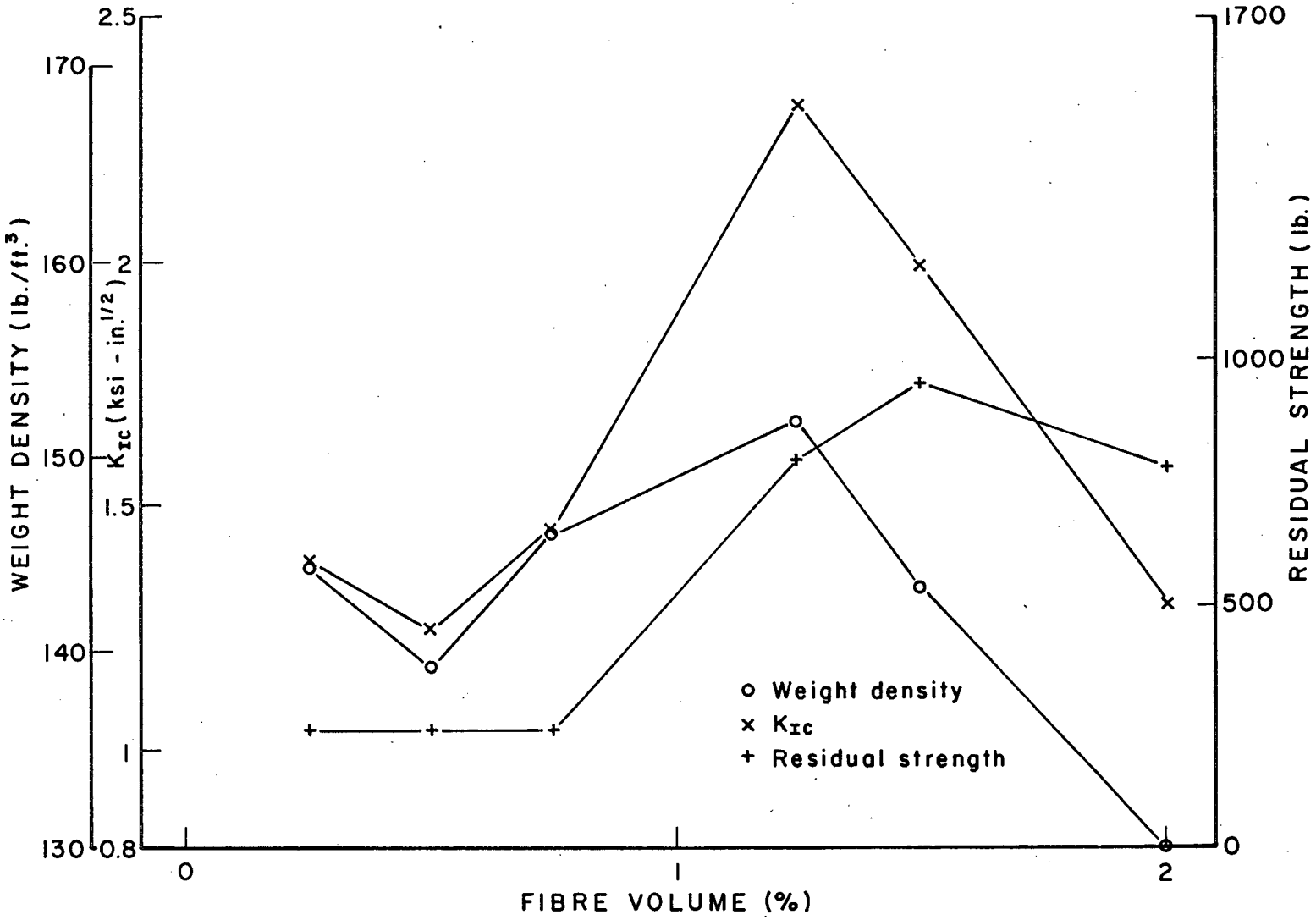

Figure 5.6 Relationships Between Fracture Toughness, Weight Density, Residual Strength and Fibre Volume for ½" SSF Series

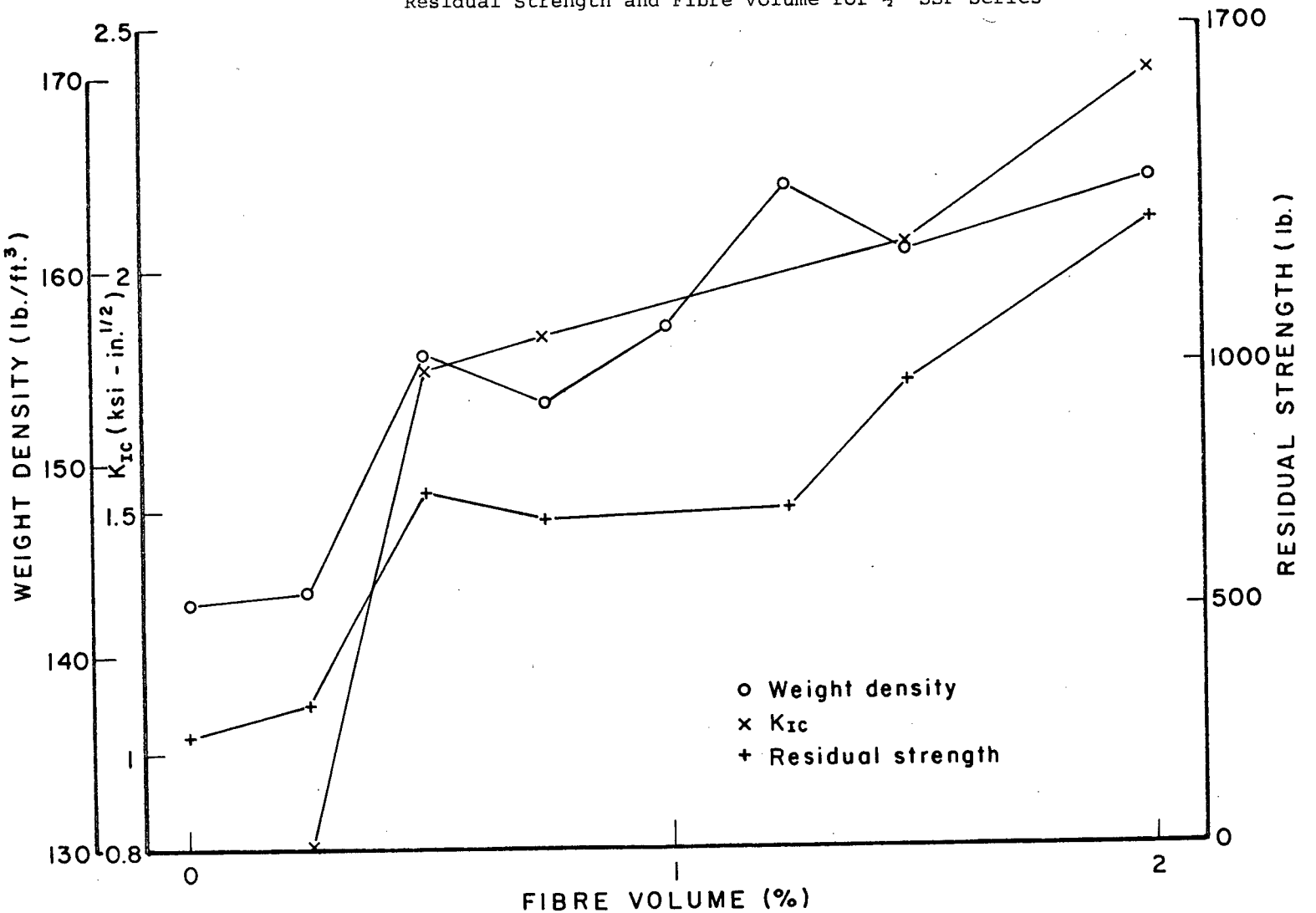

Figure 5.7 Relationships Between Fracture Toughness, Weight Density, Residual Strength and Fibre Volume for 1" SSF Series

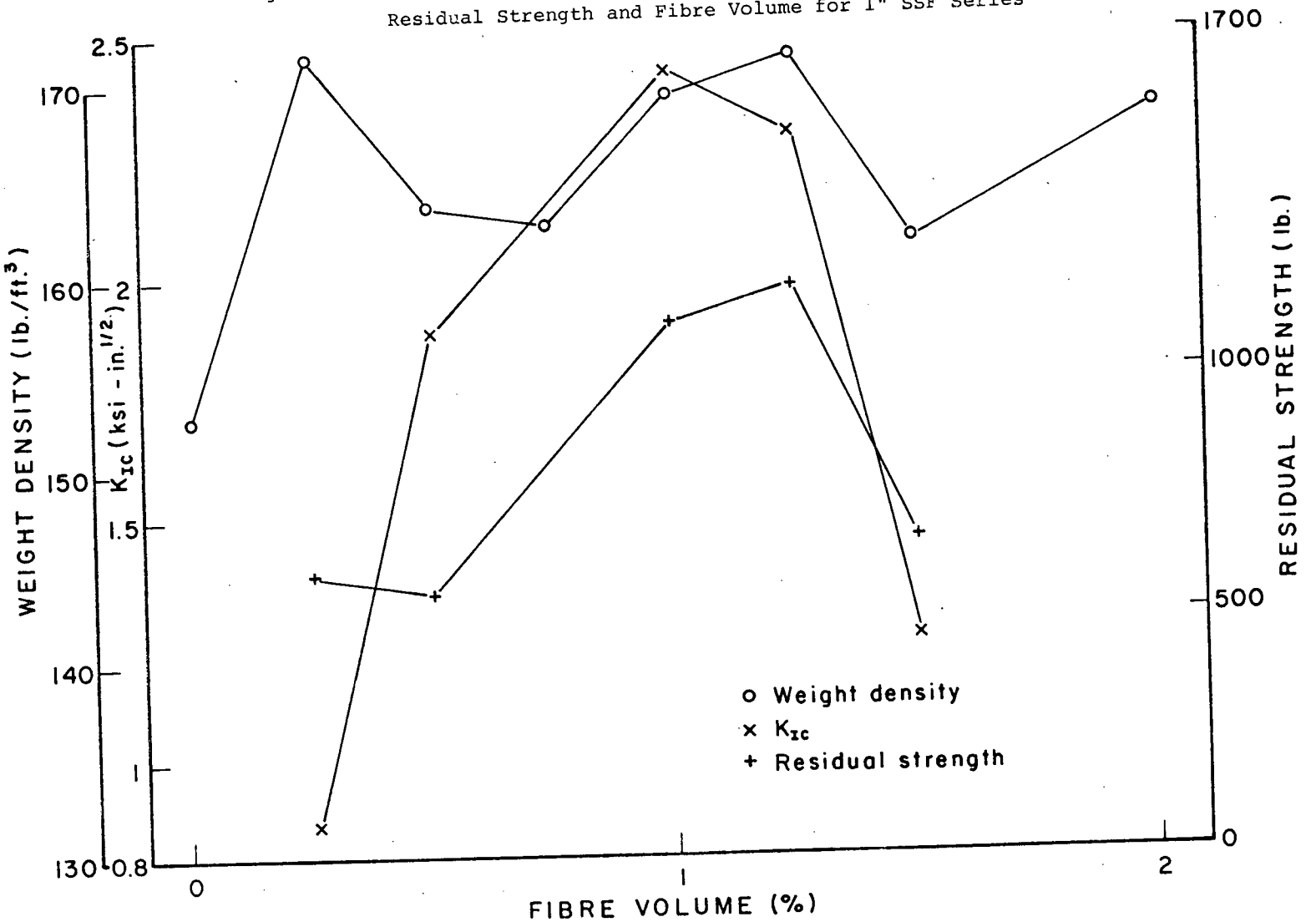

Figure 5.8 Relationships Between Fracture Toughness, Weight Density, Residual Strength and Fibre Volume for BSF Series

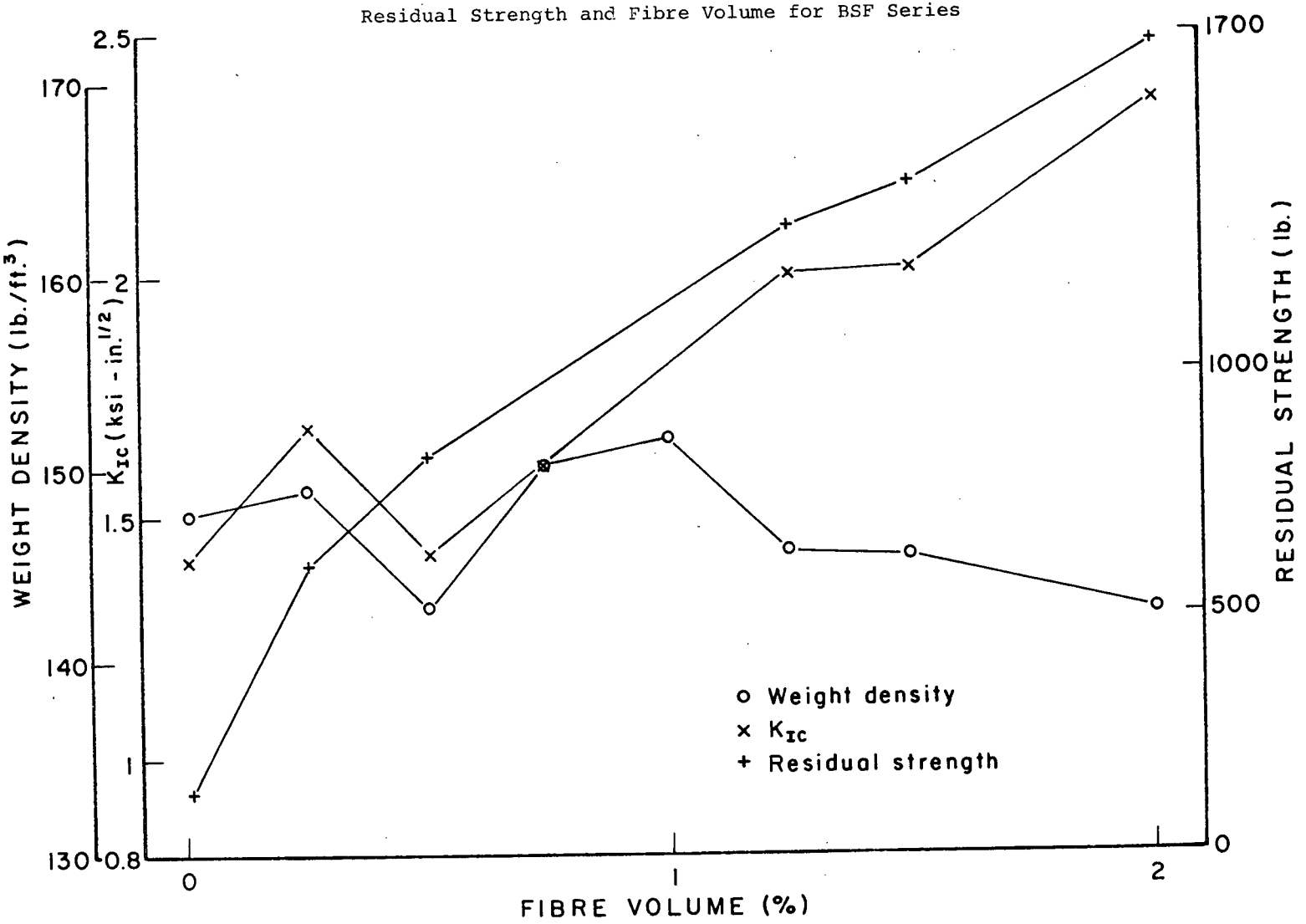

Fibre reinforced concrete is difficult to compact fully, and a poorly compacted specimen will leave voids and pores in the finished product. At the higher fibre contents, weight densities (Table 5.4) decreased due to incomplete compaction. The weight densities of the specimens are plotted against their fibre volume in Figures 5.4 to 5.8, and the degree of compaction is related directly to the weight density. The weight density curves obtained can be characterized by an inverted V. The weight density of the specimens normally increased with increasing fibre content and reached its highest value at about 1 to 1.25 per cent fibre by volume, then started to decline. In general, the shape of the fracture toughness vs fibre volume curves follows the same pattern as the weight density vs fibre volume curves. This indicates that the fracture toughness is affected by the degree of compaction of the concrete. At higher fibre contents, the trend of the fracture toughness vs fibre volume for the BSF series does not follow the same pattern as the weight density vs fibre volume curve. This disparity may be accounted for by the fact that BSF is a more efficient fibre, and the increase in fibre volume compensates for the adverse effect of the poor compaction. Thus the effect of poor compaction is less severe on the BSF series.

TABLE 5.4 WEIGHT DENSITY OF SPECIMENS

Series	Fibre Content %	Weight (lb)	Weight Density ($lb/_{ft}3$)
GF-102	0	129.1	147.0
	0.25	125.3	142.6
	0.5	121.7	138.5
	0.75	125.4	142.8
	1.0	131.5	149.7
	1.25	126.0	143.4
	2.0	123.1	140.1
GF-204	0.25	125.8	143.2
	0.5	122.5	139.4
	0.75	128.4	146.2
	1.0	127.0	144.5
	1.25	133.5	152.0
	1.5	126.0	143.4
	2.0	114.4	130.2
½"SSF	0	125.5	142.8
	0.25	125.9	143.3
	0.5	136.7	155.6
	0.75	134.5	153.1
	1.0	137.7	156.8
	1.25	144.2	164.2
	1.5	141.3	160.8
	2.0	144.4	164.4
1" SSF	0	134.1	152.7
	0.25	150.6	171.4
	0.5	143.7	163.6
	0.75	142.8	162.6
	1.0	148.8	169.4
	1.25	150.6	171.4
	1.5	142.1	161.8
	2.0	148.1	168.6
BSF	0	129.9	147.9
	0.25	130.7	148.8
	0.5	125.4	142.8
	0.75	132.0	150.3
	1.0	133.1	151.5
	1.25	128.0	145.7
	1.5	127.7	145.4
	2.0	125.2	142.5

5.4 Residual Strength

Residual strength is defined as the strength remaining after the crack has visibly extended across the entire length of the specimen. The residual strengths of the specimens are tabulated in Table 5.3, and are plotted against fibre volume together with the fracture toughness in Figures 5.4 to 5.8. The residual strength of the specimens is the combined effect of the interlocking force between aggregates and the pullout resistance of the fibre reinforcement. Zero residual strength was obtained for the two cement paste specimens. The residual strengths of the plain concrete specimens are therefore due to the interlocking of the aggregates. The pattern of these curves coincides with that of the fracture toughness curves, and the results are similarly affected by the compaction of the specimens. This is illustrated by the similar slopes of the curves. In general, as the weight density curve goes up, the fracture toughness and the residual strength curves also go up. When the weight density curves go down, so do the other two curves. The relationship between residual strength and fibre volume is shown in Figure 5.9. The difference in slopes of the residual strength vs fibre volume curves is related to the difference in pullout resistance for different types of fibres. Higher slopes generally indicate a higher pullout resistance. However, because of the scatter shown in Figure 5.9, it is difficult to assess the pullout resistance of the fibres used in this study from the available data.

Figure 5.9 Relationship Between Residual Strength and Fibre Volume

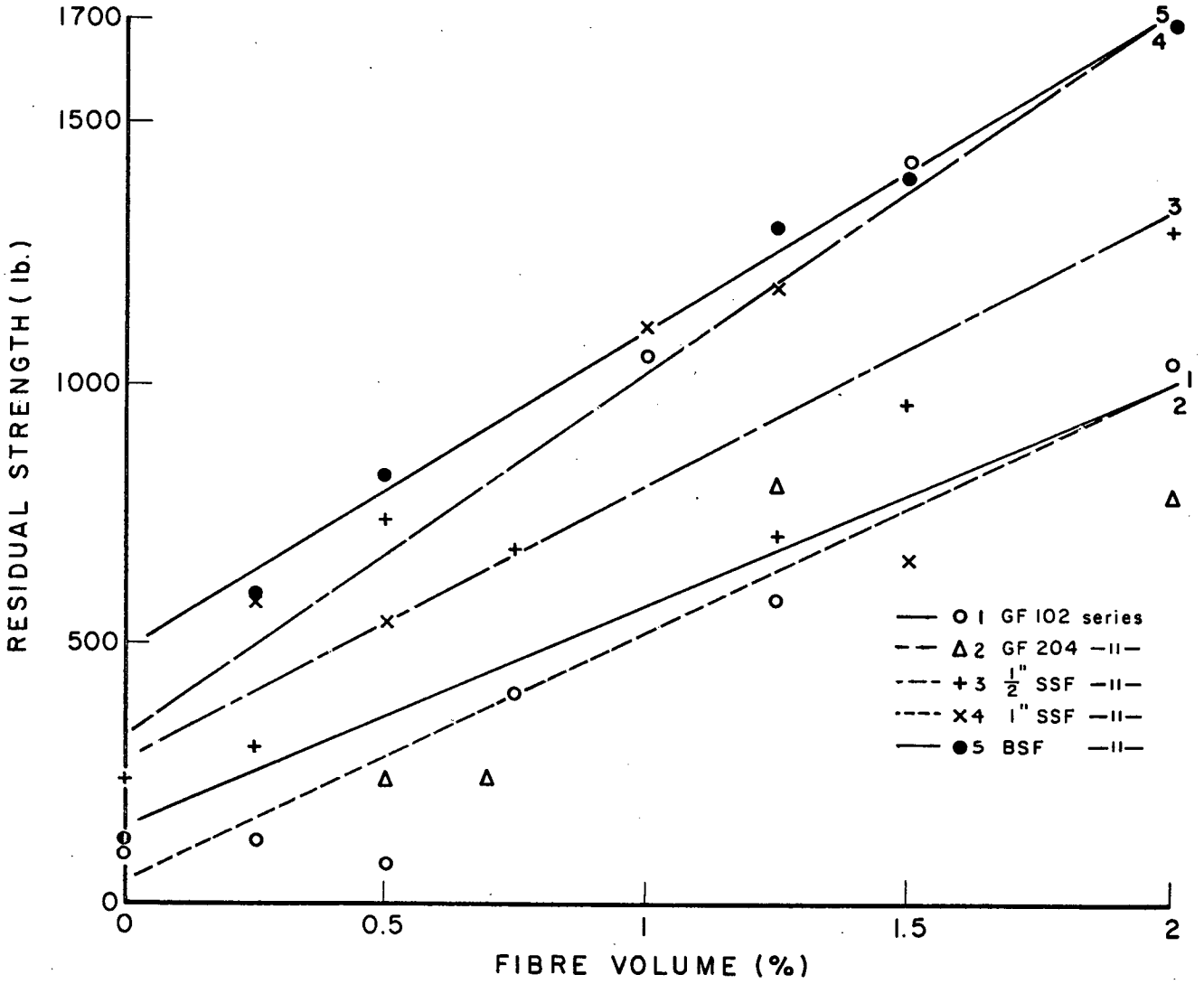

5.5 Compliance

Two specimens were used to measure the system compliance. The test results are tabulated in Tables 5.5 and 5.6, and plotted in Figure 5.10. The values of the slope and y-intercept of the compliance vs crack length curve of specimen BSF 1.0 are higher than those of the specimen ½"SSF 1.0. This implies that specimen BSF 1.0 is more compliant than specimen ½"SSF 1.0, as might be expected from the fact that the BSF 1.0 specimen also had a lower density.

5.6 V-K_I Plot

The load relaxation data are tabulated in Tables B1 to B31 (see Appendix B), and V-K_I plots on a log-log scale are shown in Figures 5.11 to 5.15. Values of the fracture toughness and the crack velocity were calculated using Equations 20 and 22 respectively. Values of the initial and final crack lengths are 4 in. (101.6 mm) and 48 in. (1219 mm). (At failure, the crack always ran right to the end of the specimen, therefore, the final crack length is always equal to 48 in. (1219 mm)). The relationships between the crack velocity and stress intensity of the specimens are summarized in Table 5.7. They were analysed using linear regression analysis. The correlation coefficients of these regression analyses ranged from 0.80 to 0.99, and they were significant at the 5% level. Therefore, a good correlation between the crack velocity and the stress intensity factor exists.

Table 5.5 Results of Compliance Study for Specimen ½" SSF

Crack length (in) a	load (kip)x10^{-1} p	Gauge Reading (in)x10^{-3} in	Gauge Reading (in)x10^{-3} out	Deflection (in)x10^{-3} y	Compliance (in/kip)x10^{-3} y/p	Average Compliance (in/kip)x10^{-3}
4	2	3	5	2	10	6.96
	4	6	9	3	7.5	
	6	10	13.2	3.2	5.3	
	8	14	18	4	5	
	10	21	28	7	7	
7	2	3	5	2	10	9.03
	4	6	9.2	3.2	8	
	6	9	14.5	5.5	9.16	
	8	12	18.8	6.8	8.5	
	10	15	24.5	9.5	9.5	
10	2	3.4	5.2	1.8	9	7.73
	4	6.1	9	2.9	7.25	
	6	8.8	13	4.2	7	
	8	11	17	6	7.5	
	10	13.1	21	7.9	7.9	
16	2	3	6.5	3.5	17.5	13.95
	4	5	10.5	5.5	13.75	
	6	7	14.8	7.8	13	
	8	8.5	18.5	10	12.5	
	10	10	23	13	13	
19	2	5	9	4	20	15.70
	4	8	14.4	6.4	16	
	6	11	19.2	8.2	13.6	
	8	13.1	24.8	11.7	14.6	
	10	15.8	30	14.2	14.2	

Table 5.6 Results of Compliance Study for Specimen BSF 1.0

Crack length (in) a	load (kip)x10^{-1} p	Gauge Reading (in)x10^{-3} in	Gauge Reading (in)x10^{-3} out	Deflection (in)x10^{-3} y	Compliance (in/kip)x10^{-3} y/p	Average Compliance (in/kip)x10^{-3}
7	2	1.5	3	1.5	7.5	9.375
	4	3	7	4	10	
	6	4	10	6	10	
	8	5	13	8	10	
10	2	2.5	5.5	3	15	13.35
	4	4.5	10	5.5	13.75	
	6	6.5	14	7.5	12.5	
	8	9	19	10	12.5	
	10	11	24	13	13	
13	2	2.5	6	3.5	17.5	15.48
	4	4.5	11	6.5	16.25	
	6	6.5	15	8.5	14.17	
	8	8	20	12	15	
	10	9.5	24	14.5	14.5	
16	2	2	5.5	3.5	17.5	17.11
	4	4.5	11.5	7	17.5	
	6	6.5	16.5	10	16.7	
	8	8	21.5	13.5	16.88	
	10	9.5	26.5	17	17	
19	2	3.5	7	3.5	17.5	18.92
	4	6	14	8	20	
	6	8	19	11	18.3	
	8	10	25	15	18.75	
	10	11	31	20	20	
22	2	2	6	4	20	19.84
	4	4.5	12	7.5	18.75	
	6	6	18	12	20	
	8	7.5	24	16.5	20.6	

Figure 5.10 Relationship Between System Compliance and Crack Length

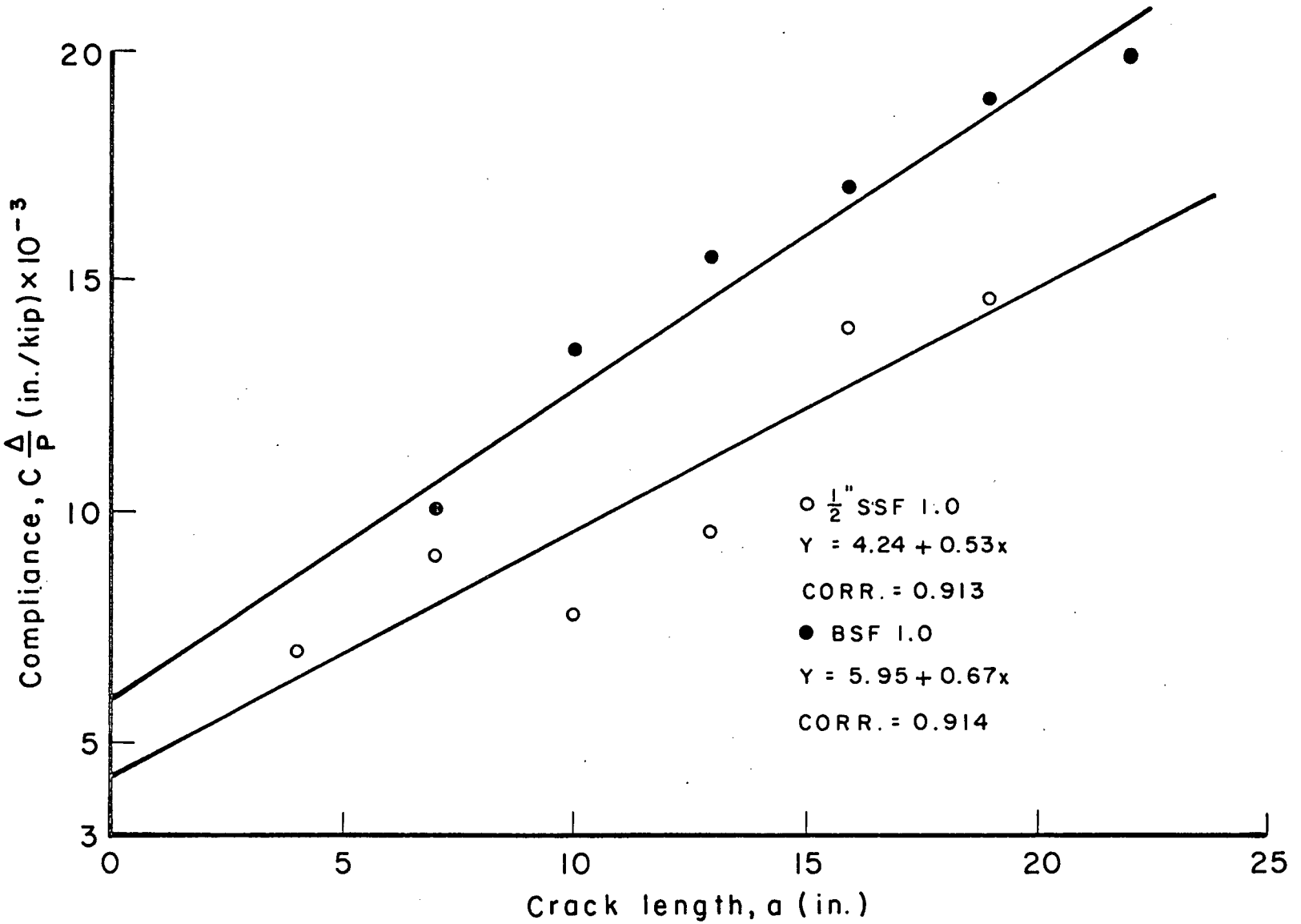

Figure 5.11 $V\text{-}K_I$ PLOTS FOR GF102 SERIES

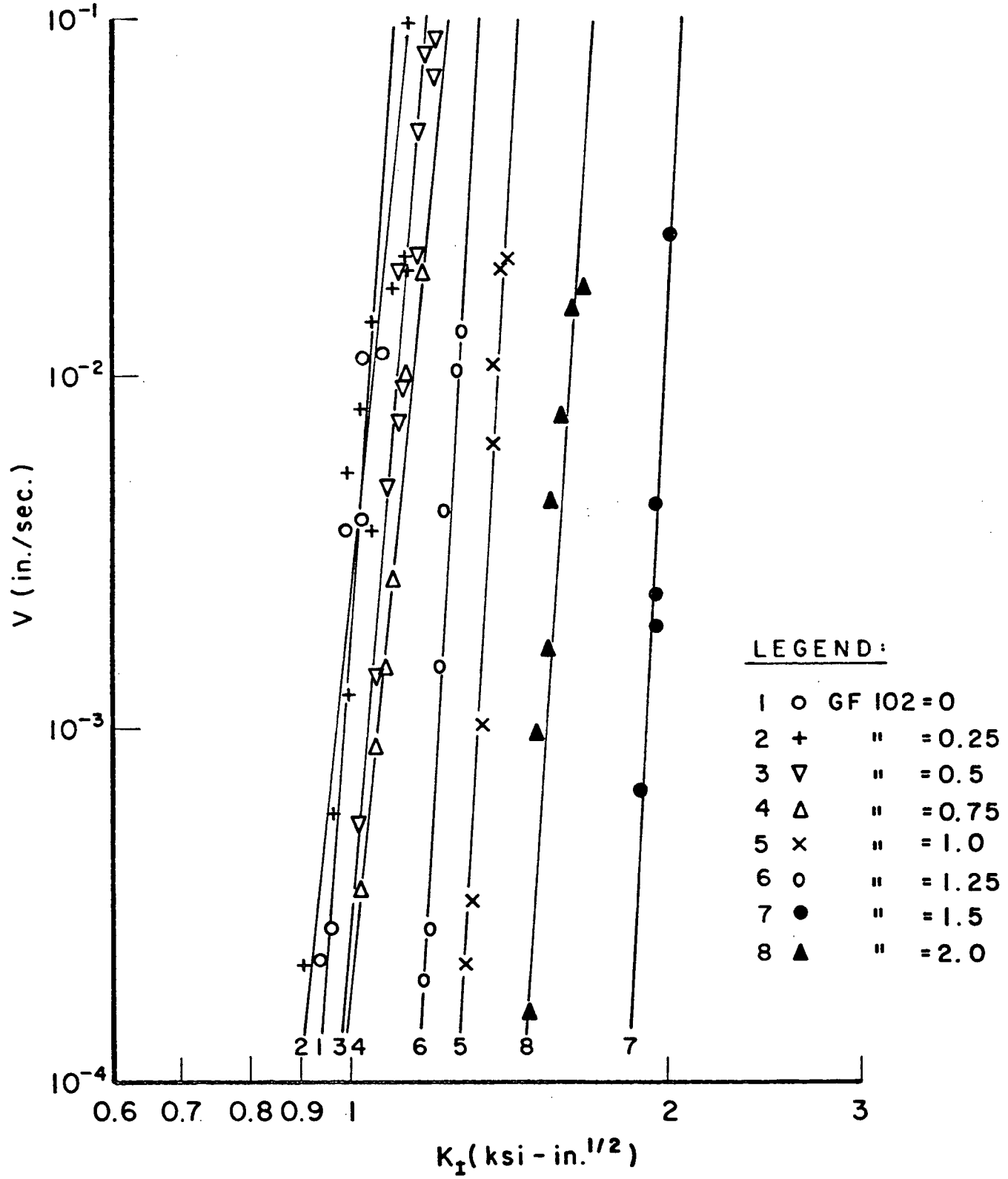

Figure 5.12 $V\text{-}K_I$ PLOTS FOR GF204 SERIES

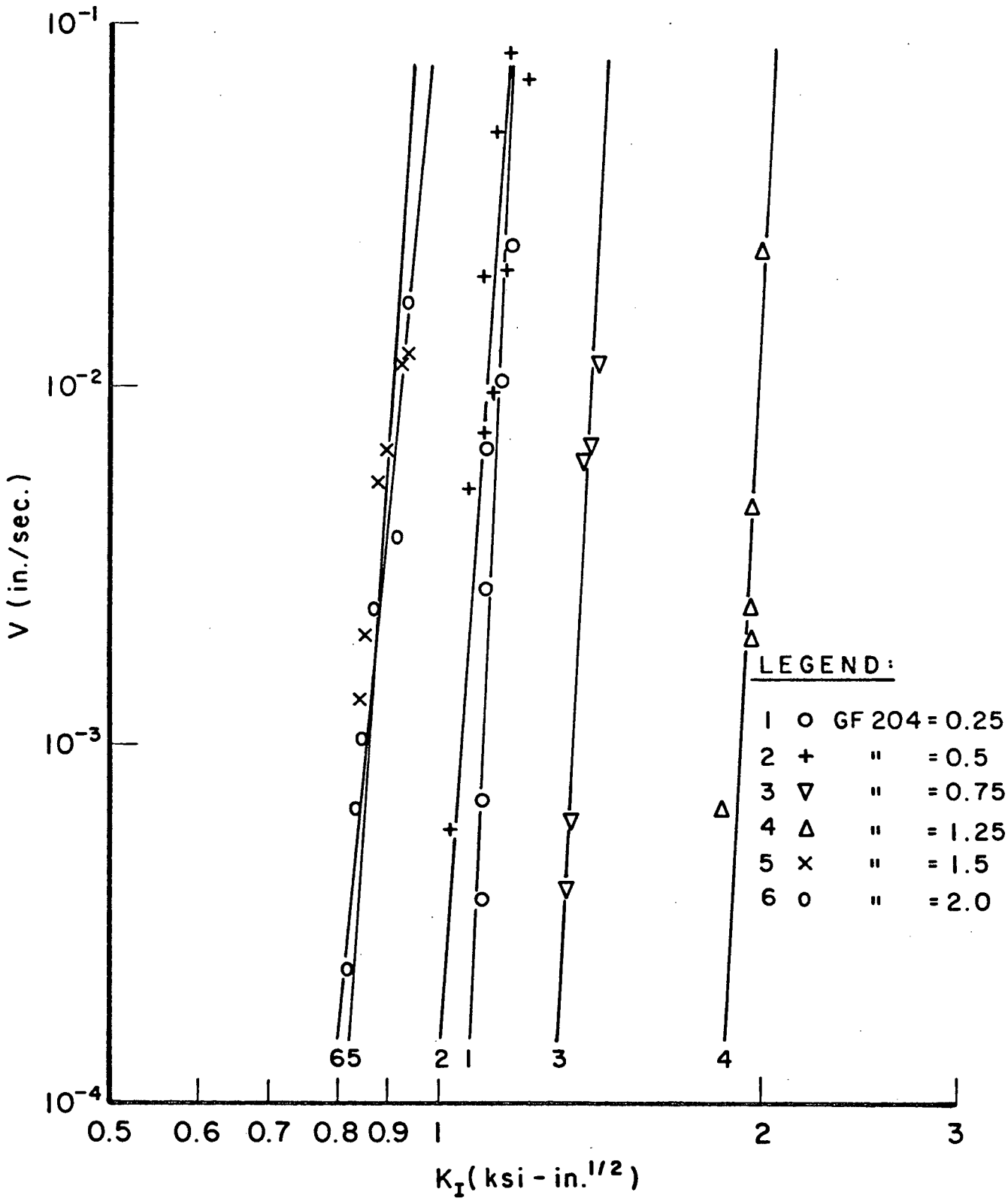

Figure 5.13 V-K_I PLOTS FOR ½" SSF SERIES

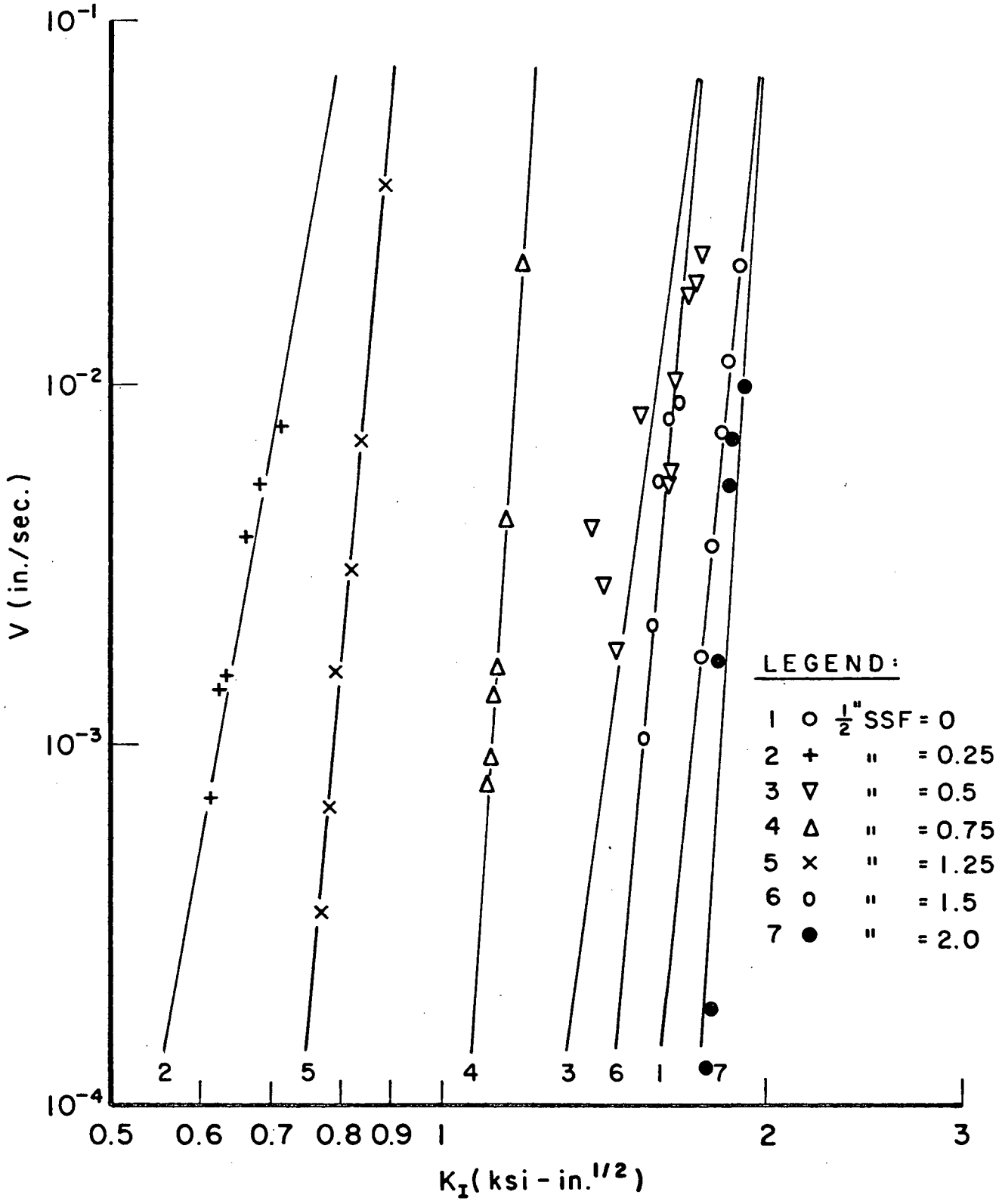

Figure 5.14 $V\text{-}K_I$ PLOTS FOR 1" SSF SERIES

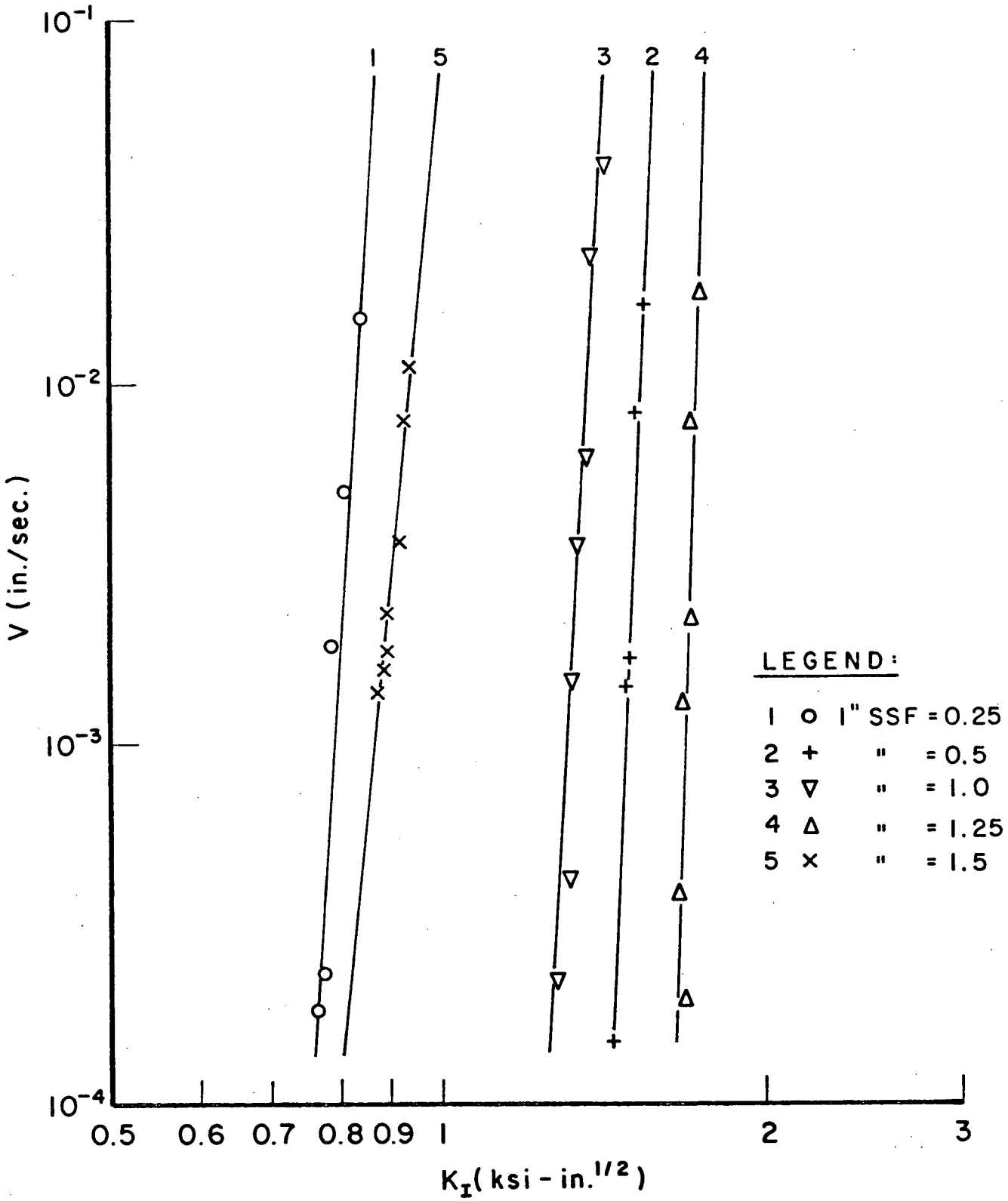

Figure 5.15 $V-K_I$ PLOTS FOR BSF SERIES

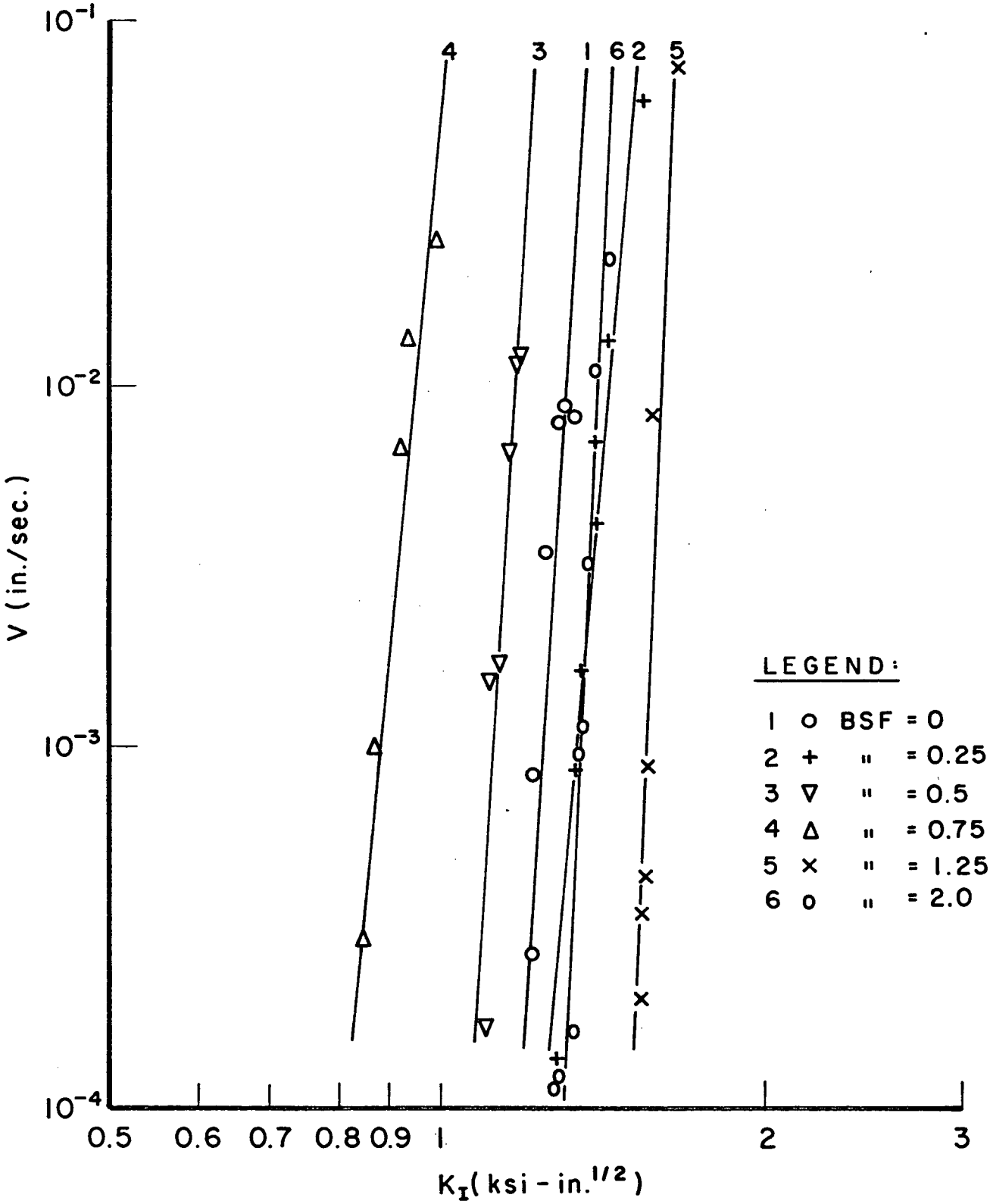

TABLE 5.7 Summary of Results for the V-K_I Curves

Mix Series	Fibre Content %	Slope n	Y-intercept A	Correlation Coefficient
GF102	0	33.3	1.35×10^{-3}	0.8
	0.25	22.4	8.39×10^{-4}	0.847
	0.5	26.5	3.16×10^{-4}	0.95
	0.75	31.6	1.3×10^{-4}	0.98
	1.0	33.8	1.02×10^{-4}	0.96
	1.25	50	5.0×10^{-8}	0.98
	1.5	33.8	3.0×10^{-12}	0.94
	2.0	41.8	2.25×10^{-11}	0.96
GF204	0.25	28.0	2.79×10^{-4}	0.99
	0.5	29.6	4.11×10^{-4}	0.96
	0.75	46.3	1.54×10^{-9}	0.96
	1.25	46	1.59×10^{-16}	0.92
	1.5	30.4	1.35×10^{-1}	0.94
	2.0	26.6	6.77×10^{-2}	0.96
½" SSF	0	29.0	2.34×10^{-10}	0.97
	0.25	16.0	2.22	0.98
	0.5	11.3	3.93×10^{-4}	0.9
	0.75	32.0	6.30×10^{-5}	0.97
	1.25	29.3	1.01	0.99
	1.5	29.9	4.03×10^{-9}	0.92
	2	63.0	7.4×10^{-20}	0.95
1"SSF	0.25	53.0	1.07×10^{-2}	0.97
	0.5	61.6	5.0×10^{-14}	0.96
	1.0	58.3	7.6×10^{-11}	0.98
	1.25	85.8	3.06×10^{-23}	0.99
	1.5	20.2	2.7×10^{-2}	0.98
BSF	0	37.1	6.62×10^{-7}	0.90
	0.25	41.1	9.7×10^{-9}	0.99
	0.5	48.6	5.98×10^{-6}	0.96
	0.75	30.9	5.56×10^{-2}	0.97
	1.25	86	4.08×10^{-20}	0.99
	2	56	7.73×10^{-11}	0.96

In Figures 5.11 to 5.15, shifting of the V-K_I curves to the right occurs as the fibre volume increases up to about 1.25 to 1.5%. No special pattern is observed after the fibre content increases to more than 1.5% of the total volume - probably due to unequal compaction. The slope of the V-K_I plots was greatest at fibre contents of 1.25%.

Chapter 6

GENERAL DISCUSSION

The results described in the previous chapter are an attempt to evaluate the effect of fibre reinforcement on crack velocity in concrete.

In the cement paste specimens, the w/c ratio was 0.4, which is lower than the 0.5 used by Nadeau, Mindess and Hay[24] and Wecharatana and Shah[27]. The value of the fracture toughness obtained in the experiment (0.69 ksi-in$^{\frac{1}{2}}$ or 0.75 MN$^{-3/2}$), was less than that obtained by Wecharatana and Shah[27] (1.2 ksi-in$^{\frac{1}{2}}$ or 1.31 MN$^{-3/2}$), but, it was twice the value obtained by Nadeau, Mindess and Hay[21] (0.293 ksi-in$^{\frac{1}{2}}$ or 0.32 MN$^{-3/2}$). However, the agreement between the slope of the V-K_I curves obtained in these tests (37.6) and the results of Nadeau, Mindess and Hay[24] (35) was good. When evaluating the fracture toughness, the size of the specimen must be large enough to accommodate the subcritical crack growth, and perhaps some amount of crack growth is needed before a "valid" K_{IC} can be obtained. These results indicate the need to define a minimum specimen size when testing cementitious materials.

The weight density of the specimen usually started to decrease when the fibre content was about 1.25% by volume. This suggests that when the fibre volume was more than 1.25%, full compaction was not achieved. Figures 5.4 to 5.8 indicated that the trend of fracture toughness curves was

similar to that of the weight density curves. The fracture toughness increased with fibre content to about 1.25%, and then decreased, due to incomplete compaction. Thus, the advantages of putting more fibre reinforcement in the specimen may be offset by the higher number of voids created due to difficulties in compaction. In the BSF series, the effect of compaction on the fracture toughness seemed to be less acute.

The slope and y-intercept are the two major parameters of the $V-K_I$ curves shown in Figures 5.11 to 5.15. A small y-intercept indicates that subcritical crack growth is less significant at low fracture toughness values. A lower slope implies that changes in fracture toughness have a small effect on the crack velocity. Therefore, for a material which is less susceptible to subcritical crack growth, the values of the y-intercept and slope of the $V-K_I$ plot should be small. Figures 5.11 to 5.15 indicate that by increasing fibre content up to about 1.25 to 1.5% of the total volume, the $V-K_I$ curves generally shifted to the right, giving a smaller y-intercept. At higher fibre contents, no pattern in the position of the $V-K_I$ curves was observed. Large slopes were generally associated with small y-intercept values. This suggests that by adding about 1.25% to 1.5% by volume of fibre reinforcement, concrete can be made less susceptible to subcritical crack growth. However,

the crack velocity is quite sensitive to changes in the fracture toughness. The fact that high fibre additions (greater than about 1.25%) do not improve the resistance to crack growth is believed to be caused by the difficulties in fully compacting the specimens. This finding is supported by the weight density results in Table 5.4.

Table 5.3 showed that the residual strength of the specimens increased as the fibre content of the specimens increased. This is probably associated with the pullout resistance of the fibre reinforcement. "Failure" of the specimen occurred when the crack propagated down the full length of the specimen. Once failure occurred, the system changed from a continuous system to a discontinuous system, consisting of two separate plates held together by fibres. Due to the loading configuration, the crack will open up at failure. This crack opening can only be accommodated if the fibres at the opening surface elongate or slip within the matrix. The fibres thus hold the specimen together after failure has occurred. Therefore, by increasing the fibre content, the residual strength of the specimens can also be increased.

Several load relaxations were performed on each specimen. Attempts were made to measure the crack position at the end of each relaxation. These included dye penetration methods and direct measurement using a magnifying glass. Both methods were found to be inadequate in measuring the true crack position.

Chapter 7

CONCLUSIONS

From the analysis of the test results, the following conclusions can be drawn:

1. Subcritical crack growth should be considered when measuring the fracture parameters of cementitious materials.
2. A minimum specimen size should be determined in order to get valid results.
3. Different types of fibre do not significantly affect the slope and intercept of the V-K_I curves.
4. The degree of compaction affects the fracture properties of the specimens. Unless special attention is given to the compaction procedure, fibre contents greater than 1.5% of the total volume are not recommended.
5. The fracture toughness increases with fibre content to about 1.25%.
6. Residual strength of the specimen increases with increasing fibre content. This strength seems also to depend on the pullout resistance of the fibre reinforcement.
7. In this test geometry, fibres do not significantly restrain crack growth.

BIBLIOGRAPHY

1. C.E. Inglis, "Stress in a Plate due to the Presence of Cracks and Sharp Corners," Trans. Institution of Naval Architect, Vol. LV, pp. 219-230 (1913).

2. H.M. Westergaard, "Bearing Pressure on Cracks," Journal of Applied Mechanics, Vol. 61, pp. A49-A53 (1939).

3. M.M. Eisenstadt, "Introduction to Mechanical Properties of Materials," The Macmillan Company, pp. 187-210 (1971).

4. A.A. Griffith, "The Phenomena of Rupture and Flow in Solids," Philosophical Transactions of Royal Society of London 226, pp. 163-198 (1920).

5. G.R. Irwin and J. Kies, "Fracturing and Fracture Dynamics," Welding Journal Research Supplement, pp. 95-100 (1952).

6. E. Orowan, "Fundamentals of Brittle Behaviour of Metals," Fatigue and Fracture of Materials, John Wiley and Sons, pp. 136-167 (1952).

7. G.C. Sih, "Handbook of Stress - Intensity Factors for Researchers and Engineers," Institute of Fracture and Solid Mechanics, Lehigh University, Bethlehem, Philadelphia (1973).

8. J.F. Knott, "Fundamentals of Fracture Mechanics," John Wiley and Sons (1973).

9. G.R. Irwin, "Linear Fracture Mechanics, Fracture Transition and Fracture Control," Engineering Fracture Mechanics, Vol. 1, No. 2, pp. 241-257 (1968)

10. D.S. Dugdale, "Experimental Study of V-Notch Fatigue Test," Journal of Mechanics and Physics of Solids, Vol. 8, NO. 2, pp. 100-104 (1960).

11. G.R. Irwin, "Plastic Zone Near a Crack and Fracture Toughness," 1960 Sagamore Ordnance Materials Conference, Syracuse University (1961).

12. W.A. Patterson and H.C. Chan, "Fracture Toughness of Glass Fibre-Reinforced Cement," Composites, Vol. 6, No. 3, pp. 102-104 (1975).

BIBLIOGRAPHY

13. A.E. Naaman, A.S. Argon and F. Moavenzaden, "A Fracture Model for Fiber Reinforced Cementitious Materials," Cement and Concrete Research, Vol. 3, No. 4, pp. 397-411 (1973).

14. F.E. Richart, A. Brandtzaeg and R.L. Brown, "A Study of the Failure of Concrete Under Combined Compressive Stresses," Bulletin No. 185, Engineering Experiment Station, University of Illinois (1928).

15. J.P. Romualdi and G.B. Batson, "Mechanics of Crack Arrest in Concrete," Journal of the Engineering Mechanics Division, American Society of Civil Engineers, Vol. 89, No. EM3, pp. 143-168 (1963).

16. S. Mindess, "The Fracture of Fibre-reinforced and Polymer Impregnated Concretes," International Journal of Cementitious Composites, Vol. 2, No. 1, pp. 3-11 (1980).

17. S. Mindess, "The Cracking and Fracture of Concrete: An Annotated Bibliography, 1928-1980," Materials Research Series Report No. 2, Department of Civil Engineering, University of British Columbia (1981).

18. K. Nishioka, S. Yamakawa, K. Hirakama and S. Akihama, "Test Method for the Evaluation of the Fracture Toughness of Steel Fibre Reinforced Concrete," RILEM Symp. 1978, Testing and Test Methods of Fibre Cement Composites, The Construction Press Ltd., Lancaster, England, pp. 87-98 (1978).

19. A.M. Brandt, "Crack Propagation Energy in Steel Fibre Reinforced Concrete," International Journal of Cement Composites, Vol. 2, No. 1, pp. 35-42 (1980).

20. G.T. Halvorsen, "J-Integral Study of Steel Fibre Reinforced Concrete," International Journal of Cement Composites, Vol. 2, No. 1, pp. 13-22 (1980).

21. G. Velazco, K. Visalvanich and S.P. Shah, "Fracture Behavior and Analysis of Fibre Reinforced Concrete Beam," Cement and Concrete Research, Vol. 10, No. 1, pp. 41-51 (1980).

22. A.G. Evans, "A Method for Evaluating the Time-dependent Failure Characteristics of Brittle Materials - and Its Application to Polycrystalline Allumina," Journal of Material Science, Vol. 7, pp. 1137-1146 (1972).

BIBLIOGRAPHY

23. D.P. Williams and A.G. Evans, "A Simple Method for Studying Slow Crack Growth," Journal of Testing and Evaluation, Vol. 1, No. 4, pp. 264-270 (1973).

24. J.S. Nadeau, S. Mindess and J.M. Hay, "Slow Crack Growth in Cement Paste," Journal of the American Ceramic Society, Vol. 57, No. 2, pp. 51-54 (1974).

25. E.R. Fuller, Jr., "An Evaluation of Double Torsion Testing - Analysis," Fracture Mechanics Applied to Brittle Materials, ASTM STP 678, S.W. Freiman, Ed., American Society for Testing and Materials, Philadelphia, pp. 3-18 (1978).

26. S.M. Wiederhorn, "Subcritical Crack Growth in Ceramics," Institute for Material Research, National Bureau of Standards, Washington (1974).

27. M. Wecharatana and S.P. Shah, "Double Torsion Tests for Studying Slow Crack Growth of Portland Cement Mortar," Cement and Concrete Research, Vol. 10, No. 6, pp. 833-844 (1980).

28. R.A. Helmuth and D.H. Turk, "Elastic Moduli of Hardened Portland Cement and Tricalcium Silicate Pastes: Effect of Porosity," Symposium on Structure of Portland Cement Paste and Concrete, Highway Research Board, SR 90, Washington D.C., pp. 135-144 (1966).

APPENDIX A

Sample Calculations

Using data obtained from specimen GF 102 - 0.25

fracture toughness (K_{IC}) ksi-in$^{\frac{1}{2}}$

use $\nu = 0.20$ after Helmuth & Turk[28]

$$K_{IC} = P_{cr}\omega_m \left(\frac{3(1+\nu)}{Wt^3 tn}\right)^{\frac{1}{2}}$$

$$= (1.03)(6.875)\left(\frac{3(1+0.20)}{(15.25)(2)^3(1)}\right)^{\frac{1}{2}}$$

$$= 1.216 \text{ ksi-in}^{\frac{1}{2}}$$

where $P_{cr} = 1.03$ kips measured

$\omega_m = 6.875$ in

$W = 15.25$ in

$t = 2$ in

$t_n = 1$ in

$\nu = 0.2$

Crack Velocity

slope of relaxation curve = 510 lb/1 in

corresponding background machine relaxation = 360 lb/1 in

paper speed = 2 in/min

corresponding applied load = 950 lb

initial crack length $a_i = 4$ in

applied load corresponding to initial crack length $P_i = 950$ lb

$$\frac{P}{t} = 510^{\#}/\text{in} \cdot 2 \text{ in/min} \cdot \frac{\text{min}}{60 \text{ sec}} - 360^{\#}/\text{in} \cdot 2 \text{ in/min} \cdot \frac{\text{min}}{60 \text{ sec}}$$

$$= 5^{\#}/\text{sec}$$

$$V = \frac{950^{\#} \cdot 4 \text{ in}}{(950^{\#})^2} \cdot 5^{\#}/\text{sec} = 0.021 \text{ in/sec}$$

APPENDIX B

TABLE B1

Load Relaxation Data for Glass Fiber

Fiber volume: 0

Load at failure: 1150 lb

Load after failure: 100 lb

Apparent Relaxation (a)					Corresponding Background Relaxation (b)				True Relaxation	Velocity	Stress Intensity
load lb p	load lb dp	paper (in) dm	time (sec) dt	slope $(\frac{dp}{dt})_b$	load lb dp	paper (in) dm	time (sec) dt	slope $(\frac{dp}{dt})_a$	$(\frac{dp}{dt})_a - (\frac{dp}{dt})_b$	$V \times 10^{-2}$ in/sec	K $\frac{1}{2}$ ksi-in
*910	300	0.75	22.5	13.33	330	1.03	30.9	10.667	2.666	1.77	1.075
880	280	1.125	33.75	7.78	240	1.5	45	5.333	2.444	1.15	1.04
860	250	2.5	75	3.333	150	2	60	2.5	0.833	0.41	1.015
840	82	2.25	67.5	1.215	120	3.5	105	1.143	0.0721	0.37	0.99
820	70	4	120	0.583	40	2.5	75	0.533	0.05	0.027	0.968
800	38	5.5	160	0.23	30	5.5	165	0.182	0.049	0.025	0.94

*Initial Load

TABLE B2

Load Relaxation Data for Glass Fiber size 102 series

Fiber volume: 0.25%

Load at failure: 1030 lb

Load after failure: 120 lb

Apparent Relaxation (a)					Corresponding Background Relaxation (b)				True Relaxation	Velocity	Stress Intensity
load lb p	load lb dp	paper (in) dm	time (sec) dt	slope $(\frac{dp}{dt})_b$	load lb dp	paper (in) dm	time (sec) dt	slope $(\frac{dp}{dt})_a$	$(\frac{dp}{dt})_a - (\frac{dp}{dt})_b$	$V \times 10^{-2}$ in/sec	K $\frac{1}{2}$ ksi-in
*950	510	1	30	17	360	1	30	12	5	2.1	1.15
900	560	2.5	75	7.46	360	2.5	75	4.4	3.067	1.43	1.089
880	240	2.5	75	3.2	160	3.5	105	1.52	168	0.824	1.065
860	100	2	60	1.66	80	4.5	135	0.593	1.07	0.549	1.04
840	100	4	120	0.833	80	4.5	135	0.593	0.24	0.13	1.014
820	40	4.5	135	0.296	20	3.5	105	0.19	0.106	0.06	0.99
800	20	6	180	0.111	10	4.5	135	0.074	0.037	0.022	0.963
a 1030	470	1	30	15.6	360	1	30	12	3.66	14.2	1.246
980	300	2.5	75	4	160	3.5	105	1.52	2.44	10.6	1.18
960	120	2	60	2	160	3.5	105	1.52	0.48	2.15	1.15
940	100	3.31	99	1	80	4.5	135	0.593	0.413	1.93	1.14
920	60	3	90	0.67	80	4.5	135	0.593	0.077	0.375	1.11
900	140	2.5	75	1.86	20	3.5	105	0.19	1.67	0.085	1.09

*Initial Load Initial Crack Length 4 in

a Final Load Final Crack Length 48 in

TABLE B3

Load Relaxation Data for Glass Fiber size 102 series

Fiber volume: 0.5%

Load at failure: 1040 lb

Load after failure: 80 lb

Apparent Relaxation (a)					Corresponding Background Relaxation (b)				True Relaxation	Velocity	Stress Intensity
load lb p	load lb dp	paper (in) dm	time (sec) dt	slope $(\frac{dp}{dt})_b$	load lb dp	paper (in) dm	time (sec) dt	slope $(\frac{dp}{dt})_a$	$(\frac{dp}{dt})_a - (\frac{dp}{dt})_b$	$V \times 10^{-2}$ in/sec	K ksi-in$^{\frac{1}{2}}$
*1000	380	1	60	12.66	380	1.818	54.38	6.98	5.68	2.2	1.18
960	300	2	60	5	140	1.688	50.63	2.76	2.24	0.95	1.15
940	80	0.938	28.1	2.84	70	2	60	1.167	1.67	0.757	1.11
920	60	1.375	41.25	1.45	50	4.5	135	0.37	1.08	0.51	1.086
900	60	3	180	0.667	50	4.5	135	0.37	0.296	0.146	1.063
880	40	6	180	0.222	30	9	270	0.111	0.111	0.057	1.04

*Initial Load

TABLE B4

Load Relaxation Data for Glass Fiber size 102 series

Fiber volume: 0.75%

Load at failure: 1340 lb

Load after failure: 400 lb

Apparent Relaxation (a)					Corresponding Background Relaxation (b)				True Relaxation	Velocity	Stress Intensity
load lb p	load lb dp	paper (in) dm	time (sec) dt	slope $(\frac{dp}{dt})_b$	load lb dp	paper (in) dm	time (sec) dt	slope $(\frac{dp}{dt})_a$	$(\frac{dp}{dt})_a - (\frac{dp}{dt})_b$	$V \times 10^{-2}$ in/sec	K ksi-in$^{\frac{1}{2}}$
*1000	640	1.5	45	14.2	420	1.5	45	9.333	4.88	1.95	1.18
960	340	2	60	5.66	100	1	30	3.33	2.333	1.01	1.13
940	60	1	30	2	90	2.125	63.75	1.41	0.59	0.267	1.11
920	40	1.5	45	0.888	50	3	90	0.555	0.333	0.157	1.08
900	40	3.5	105	0.381	20	3.5	105	0.19	0.191	0.094	1.06
880	20	4	120	0.167	20	7	210	0.095	0.072	0.037	1.04

*Initial Load

TABLE B5

Load Relaxation Data for Glass Fiber size 102 series

Fiber volume: 1.0%

Load at failure: 1600 lb.

Load after failure: 1050 lb

Apparent Relaxation (a)					Corresponding Background Relaxation (b)				True Relaxation	Velocity	Stress Intensity
load lb p	load lb dp	paper (in) dm	time (sec) dt	slope $(\frac{dp}{dt})_b$	load lb dp	paper (in) dm	time (sec) dt	slope $(\frac{dp}{dt})_a$	$(\frac{dp}{dt})_a - (\frac{dp}{dt})_b$	$V \times 10^{-2}$ in/sec	K ksi-in$^{\frac{1}{2}}$
*1000	240	0.56	16.8	14.8	380	1.5	45	8.44	5.78	2.07	1.18
970	210	0.875	26	8	180	1.75	52.5	3.43	4.51	1.9	1.146
960	150	1.625	48.8	3.08	80	1	30	0.688	1.497	0.65	1.134
940	40	1	30	1.333	40	1.75	52.5	0.762	0.57	0.25	1.11
910	50	3	90	0.555	30	4	120	0.25	0.305	0.147	1.07
900	40	6	180	0.222	20	6	180	0.111	0.111	0.0548	1.06

*Initial Load

TABLE B6

Load Relaxation Data for Glass Fiber size 102 series

Fiber volume: 1.25%

Load at failure: 1680 lb

Load after failure: 580 lb

Apparent Relaxation (a)					Corresponding Background Relaxation (b)				True Relaxation	Velocity	Stress Intensity
load lb p	load lb dp	paper (in) dm	time (sec) dt	slope $(\frac{dp}{dt})_b$	load lb dp	paper (in) dm	time (sec) dt	slope $(\frac{dp}{dt})_a$	$(\frac{dp}{dt})_a - (\frac{dp}{dt})_b$	$V \times 10^{-2}$ in/sec	K $\frac{1}{2}$ ksi-in
*1100	205	0.438	13.13	15.62	520	1.5	45	11.55	4.07	1.49	1.292
1080	380	1.5	45	8.44	320	1.94	58.2	5.50	2.94	1.1	1.275
1060	180	1.5	45	4	280	3.25	97.5	2.887	1.113	0.433	1.25
1040	180	3.5	105	1.71	150	3.75	112.5	1.33	0.384	0.155	1.223
1020	60	4.81	144.3	0.416	50	4.75	142.5	0.35	0.0646	0.027	1.204
1000	40	7.75	232.5	0.172	20	6	180	0.111	0.0609	0.026	1.18

*Initial Load

TABLE B7

Load Relaxation Data for Glass Fiber size 102 series

Fiber volume: 1.5%

Load at failure: 2000 lb

Load after failure: 1420 lb

Apparent Relaxation (a)					Corresponding Background Relaxation (b)				True Relaxation	Velocity	Stress Intensity
load lb p	load lb dp	paper (in) dm	time (sec) dt	slope $(\frac{dp}{dt})_b$	load lb dp	paper (in) dm	time (sec) dt	slope $(\frac{dp}{dt})_a$	$(\frac{dp}{dt})_a - (\frac{dp}{dt})_b$	$V \times 10^{-2}$ in/sec	K ksi-in$^{\frac{1}{2}}$
*1600	400	1	30	13.33	680	2	60	11.33	2	0.5	1.89
1560	480	2.78	83.4	5.75	420	3	90	4.67	1.08	0.28	1.84
1540	380	4.688	140.6	270	260	4.44	133	1.95	0.747	0.20	1.82
1520	80	1.75	52.5	1.52	160	5	150	1.067	0.457	0.126	1.79
1500	100	4	120	0.833	60	4	120	0.5	0.33	0.094	1.77
1480	60	4.5	13.5	0.444	30	5.75	172.5	0.174	0.27	0.079	1.75
1460	40	6	180	0.222	30	5.75	172.5	0.174	0.048	0.014	1.72

*Initial Load

TABLE B8

Load Relaxation Data for Glass Fiber size 102 series

Fiber volume: 2.0%

Load at failure: 1500 lb

Load after failure: 1040 lb

Apparent Relaxation (a)					Corresponding Background Relaxation (b)				True Relaxation	Velocity	Stress Intensity
load lb p	load lb dp	paper (in) dm	time (sec) dt	slope $(\frac{dp}{dt})_b$	load lb dp	paper (in) dm	time (sec) dt	slope $(\frac{dp}{dt})_a$	$(\frac{dp}{dt})_a - (\frac{dp}{dt})_b$	$V \times 10^{-2}$ in/sec	K $\frac{1}{2}$ ksi-in
*1400	440	1	30	14.66	500	2	60	8.333	6.33	1.81	1.65
1380	430	1.5	45	9.555	200	1.5	45	4.44	5.111	1.48	1.63
1340	140	1	30	4.667	140	2.125	63.75	2.196	2.47	0.77	1.58
1320	120	2	60	2	80	2.938	88.13	0.908	1.09	0.35	1.56
1300	60	2.25	67.5	0.885	50	4.5	135	0.37	0.519	0.17	1.535
1280	80	6	180	0.444	30	7	210	0.143	0.301	0.102	1.51
1260	40	7	210	0.19	20	9.5	285	0.0701	0.047	0.016	1.488

*Initial Load

TABLE B9

Load Relaxation Data for Glass Fiber size 204 series

Fiber volume: 0.25%

Load at failure: 1150 lb

Load after failure: 240 lb

Apparent Relaxation (a)					Corresponding Background Relaxation (b)				True Relaxation	Velocity	Stress Intensity
load lb p	load lb dp	paper (in) dm	time (sec) dt	slope $(\frac{dp}{dt})_b$	load lb dp	paper (in) dm	time (sec) dt	slope $(\frac{dp}{dt})_a$	$(\frac{dp}{dt})_a - (\frac{dp}{dt})_b$	$V \times 10^{-2}$ in/sec	K $\frac{1}{2}$ ksi-in
*1000	440	1	30	14.67	260	1	30	8.667	6	2.4	1.18
970	340	1.5	45	7.55	160	1.06	31.8	5.02	2.535	1.07	1.14
940	140	1.375	41.3	3.39	100	1.75	52.5	1.905	1.492	0.675	1.11
920	120	3	90	1.333	80	3.5	105	0.762	0.571	0.27	1.08
880	40	2.75	82.5	0.485	30	3	90	0.33	0.152	0.078	1.04
860	20	3.75	112.5	0.178	20	6	180	0.111	0.067	0.038	1.015

*Initial Load

TABLE B10

Load Relaxation Data for Glass Fiber size 204 series

Fiber volume: 0.75%

Load at failure: 1400 lb

Load after failure: 244 lb

Apparent Relaxation (a)					Corresponding Background Relaxation (b)				True Relaxation	Velocity	Stress Intensity
load lb p	load lb dp	paper (in) dm	time (sec) dt	slope $(\frac{dp}{dt})_b$	load lb dp	paper (in) dm	time (sec) dt	slope $(\frac{dp}{dt})_a$	$(\frac{dp}{dt})_a - (\frac{dp}{dt})_b$	$V \times 10^{-2}$ in/sec	K ksi-in$^{\frac{1}{2}}$
*1200	600	1	30	20	500	1	30	1.667	3.333	1.11	1.417
1180	270	0.813	24.4	11.07	280	1.031	31	9.05	2.02	0.696	1.39
1140	140	2.812	84.4	6	200	1.563	46.9	4.267	1.733	0.64	1.37
1130	90	2	60	1.5	120	3	90	1.33	0.167	0.062	1.33
1110	50	2.75	82.5	0.606	60	4	120	0.5	0.106	0.04	1.31

*Initial Load

TABLE B11

Load Relaxation Data for Glass Fiber size 204 series

Fiber volume: 1.25%

Load at failure: 1920 lb

Load after failure: 800 lb

Apparent Relaxation (a)					Corresponding Background Relaxation (b)				True Relaxation	Velocity	Stress Intensity
load lb p	load lb dp	paper (in) dm	time (sec) dt	slope $(\frac{dp}{dt})_b$	load lb dp	paper (in) dm	time (sec) dt	slope $(\frac{dp}{dt})_a$	$(\frac{dp}{dt})_a - (\frac{dp}{dt})_b$	$V \times 10^{-2}$ in/sec	K ksi-in$^{\frac{1}{2}}$
*1700	720	1	30	24	410	1	30	13.67	10.33	2.43	2.0
1680	520	1.5	45	11.55	290	1	30	9.67	1.885	0.454	1.98
1650	270	2	60	4.5	210	2	60	3.5	0.993	0.248	1.95
1640	240	3	90	2.66	308	2.75	165	1.866	0.794	0.2	1.94
1580	40	3.25	97.5	0.41	20	4	120	0.167	0.243	0.066	1.867

* Initial Load

TABLE B12

Load Relaxation Data for Glass Fiber size 204 series

Fiber volume: 1.5%

Load at failure: 1660 lb

Load after failure: 960 lb

Apparent Relaxation (a)					Corresponding Background Relaxation (b)				True Relaxation	Velocity	Stress Intensity
load lb p	load lb dp	paper (in) dm	time (sec) dt	slope $(\frac{dp}{dt})_b$	load lb dp	paper (in) dm	time (sec) dt	slope $(\frac{dp}{dt})_a$	$(\frac{dp}{dt})_a - (\frac{dp}{dt})_b$	$V \times 10^{-2}$ in/sec	K ksi-in$^{\frac{1}{2}}$
*800	500	1.5	45	11.11	260	1	30	8.667	2.444	1.22	0.945
780	410	2	60	6.83	280	2	60	4.617	2.167	1.139	0.921
760	280	2.5	75	3.73	150	2	60	2.5	1.23	0.68	0.897
750	120	2	60	2	90	2.75	82.5	1.09	0.91	0.517	0.886
730	60	3	90	0.667	60	6.25	187.5	0.32	0.346	0.208	0.86
720	40	6	180	0.222	20	14.5	435	0.046	0.176	0.137	0.85
700	20	10	300	0.066	20	14.5	435	0.046	0.02	0.014	0.82

*Initial Load

TABLE B13

Load Relaxation Data for Glass Fiber size 204 series

Fiber volume: 2.0%

Load at failure: 1080 lb

Load after failure: 780 lb

Apparent Relaxation (a)					Corresponding Background Relaxation (b)				True Relaxation	Velocity	Stress Intensity
load lb p	load lb dp	paper (in) dm	time (sec) dt	slope $(\frac{dp}{dt})_b$	load lb dp	paper (in) dm	time (sec) dt	slope $(\frac{dp}{dt})_a$	$(\frac{dp}{dt})_a - (\frac{dp}{dt})_b$	$V \times 10^{-2}$ in/sec	K ksi-in$^{\frac{1}{2}}$
*800	380	1	30	12.667	140	0.5	15	9.333	3.333	1.667	0.945
770	230	1.31	39.34	5.84	300	1.94	58.1	5.16	0.68	0.367	0.909
740	360	3.5	105	2.476	186	3	90	2.067	0.409	0.239	0.874
720	100	3.5	105	0.952	100	4.25	127.5	0.784	0.168	0.104	0.838
700	20	5.5	165	0.121	10	4	120	0.083	0.038	0.025	0.826

*Initial Load

TABLE B14

Load Relaxation Data for Straight Steel Fiber

Fiber volume: 0

Load at failure: 1860 lb

Load after failure: 240 lb

Apparent Relaxation (a)					Corresponding Background Relaxation (b)				True Relaxation	Velocity	Stress Intensity
load lb p	load lb dp	paper (in) dm	time (sec) dt	slope $(\frac{dp}{dt})_b$	load lb dp	paper (in) dm	time (sec) dt	slope $(\frac{dp}{dt})_a$	$(\frac{dp}{dt})_a - (\frac{dp}{dt})_b$	$V \times 10^{-2}$ in/sec	K $\frac{1}{2}$ ksi-in
*1600	236	0.5	15	15.7	450	2	60	7.5	8.25	2.05	1.89
1560	680	3	90	7.555	400	4	120	3.333	4.22	1.111	1.84
1520	300	2.5	75	4	140	3.31	99.3	1.408	2.592	0.718	1.79
1500	100	2	60	1.667	80	5.5	165	0.485	1.182	0.336	1.77
1480	100	4	120	0.833	40	5.5	165	0.242	0.59	0.172	1.74

*Initial Load

TABLE B15

Load Relaxation Data for 1/2" Straight Steel Fiber Series

Fiber volume: 0.25%

Load at failure: 670 lb

Load after failure: 300 lb

Apparent Relaxation (a)					Corresponding Background Relaxation (b)				True Relaxation	Velocity	Stress Intensity
load lb p	load lb dp	paper (in) dm	time (sec) dt	slope $(\frac{dp}{dt})_b$	load lb dp	paper (in) dm	time (sec) dt	slope $(\frac{dp}{dt})_a$	$(\frac{dp}{dt})_a - (\frac{dp}{dt})_b$	$V \times 10^{-2}$ in/sec	K ksi-in$^{\frac{1}{2}}$
*600	280	1	30	9.333	260	1.06	31.88	8.151	1.18	0.78	0.708
580	240	2.5	75	3.2	110	1.5	45	2.44	0.76	0.54	0.685
560	120	3.5	105	1.143	40	2	60	0.667	0.46	0.364	0.66
540	40	3	90	0.443	30	4	120	0.25	0.194	0.159	0.638
530	20	2.75	82.5	0.223	8	5.25	157.5	0.051	0.172	0.146	0.625
510	8	2	60	0.133	8	5.25	157.5	0.051	0.083	0.073	0.614

*Initial Load

TABLE B16

Load Relaxation Data for 1/2" Straight Steel Fiber Series

Fiber volume: 0.5%

Load at failure: 1490 lb

Load after failure: 740 lb

Apparent Relaxation (a)					Corresponding Background Relaxation (b)				True Relaxation	Velocity	Stress Intensity
load lb p	load lb dp	paper (in) dm	time (sec) dt	slope $(\frac{dp}{dt})_b$	load lb dp	paper (in) dm	time (sec) dt	slope $(\frac{dp}{dt})_a$	$(\frac{dp}{dt})_a - (\frac{dp}{dt})_b$	$V \times 10^{-2}$ in/sec	K ksi-in$^{\frac{1}{2}}$
*1490	700	1	30	23.3	520	1.5	45	11.56	11.77	24.37	1.75
1450	250	0.5	15	16.67	240	1	30	8	8.6	18.65	1.71
1440	520	1.5	45	11.55	280	2.5	75	3.73	7.8	17.3	1.70
1400	440	2.5	75	5.86	100	2.28	8.44	1.46	4.4	10.23	1.65
1370	330	3.5	105	3.143	70	2.5	75	0.93	2.21	5.37	1.62
1280	200	1.5	45	4.44	70	2.5	75	0.93	3.51	8.4	1.512
1220	540	2.59	77.7	6.95	20	5	150	0.133	6.0	1.838	1.44

*Initial Load

TABLE B17

Load Relaxation Data for 1/2" Straight Steel Fiber Series
Fiber volume: 0.75%
Load at failure: 1540 lb
Load after failure: 680 lb

Apparent Relaxation (a)					Corresponding Background Relaxation (b)				True Relaxation	Velocity	Stress Intensity
load lb p	load lb dp	paper (in) dm	time (sec) dt	slope $(\frac{dp}{dt})_b$	load lb dp	paper (in) dm	time (sec) dt	slope $(\frac{dp}{dt})_a$	$(\frac{dp}{dt})_a - (\frac{dp}{dt})_b$	$V \times 10^{-2}$ in/sec	K $\frac{1}{2}$ ksi-in
*1000	490	1	30	16.33	150	0.5	15	10	6.33	2.3	1.19
970	360	2	60	6	300	2	60	5	1	0.43	1.145
950	170	2.5	75	2.26	340	6	180	1.88	0.386	0.17	1.122
940	80	2.5	75	1.06	80	3.5	105	0.762	0.305	0.14	1.11
920	40	2.5	75	0.533	20	2	60	0.333	0.2	0.095	1.08
910	40	4.5	135	0.296	10	2.5	75	0.133	0.165	0.08	1.075

*Initial Load

TABLE B18

Load Relaxation Data for 1/2" Straight Steel Fiber Series

Fiber volume: 1.25%

Load at failure: 780 lb

Load after failure: 700 lb

Apparent Relaxation (a)					Corresponding Background Relaxation (b)				True Relaxation	Velocity	Stress Intensity
load lb p	load lb dp	paper (in) dm	time (sec) dt	slope $(\frac{dp}{dt})_b$	load lb dp	paper (in) dm	time (sec) dt	slope $(\frac{dp}{dt})_a$	$(\frac{dp}{dt})_a - (\frac{dp}{dt})_b$	$V \times 10^{-2}$ in/sec	K ksi-in$^{\frac{1}{2}}$
*750	490	1.5	45	10.89	200	1.5	45	4.45	6.44	8.44	0.886
720	340	2	60	5.667	200	1.5	45	4.45	1.22	0.706	0.85
700	120	2	60	2	190	4.25	127.5	1.5	0.5	0.306	0.826
670	60	3.5	105	0.857	60	3.25	97.5	0.6	0.258	0.16	0.79
660	40	5	150	0.267	40	8	240	0.167	0.1	0.069	0.78
650	20	6	180	0.111	10	5.5	164	0.061	0.05	0.036	0.767

*Initial Load

TABLE B19

Load Relaxation Data for 1/2" Straight Steel Fiber Series

Fiber volume: 1.50%

Load at failure: 1700 lb

Load after failure: 960 lb

Apparent Relaxation (a)					Corresponding Background Relaxation (b)				True Relaxation	Velocity	Stress Intensity
load lb p	load lb dp	paper (in) dm	time (sec) dt	slope $(\frac{dp}{dt})_b$	load lb dp	paper (in) dm	time (sec) dt	slope $(\frac{dp}{dt})_a$	$(\frac{dp}{dt})_a - (\frac{dp}{dt})_b$	$V \times 10^{-2}$ in/sec	K ksi-in$^{\frac{1}{2}}$
*1400	740	1.5	45	16.44	200	0.5	15	13.33	3.11	3.11	1.65
1360	660	3	90	7.33	540	4.31	129.38	2.63	2.63	0.82	1.606
1340	460	4.5	135	3.4	180	3.5	105	1.71	1.59	0.527	1.58
1320	100	2.5	75	1.333	80	4	120	0.667	0.667	0.214	1.56
1300	80	4.81	144.38	0.554	20	3	90	0.222	0.332	0.11	1.535

*Initial Load

TABLE B20

Load Relaxation Data for 1/2" Straight Steel Fiber Series

Fiber volume: 2.0%

Load at failure: 1980 lb

Load after failure: 1290 lb

Apparent Relaxation (a)					Corresponding Background Relaxation (b)				True Relaxation	Velocity	Stress Intensity
load lb p	load lb dp	paper (in) dm	time (sec) dt	slope $(\frac{dp}{dt})_b$	load lb dp	paper (in) dm	time (sec) dt	slope $(\frac{dp}{dt})_a$	$(\frac{dp}{dt})_a - (\frac{dp}{dt})_b$	$V \times 10^{-2}$ in/sec	K ksi-in$^{\frac{1}{2}}$
*1600	580	1	30	19.3	582	1.25	37.5	15.47	3.866	0.967	1.89
1570	460	1.75	52.5	8.76	340	1.875	56.25	6.04	2.72	0.707	1.85
1550	360	2.25	67.5	5.33	200	2	60	3.33	2	0.532	1.83
1520	200	2.5	75	2.666	100	3.75	112.5	2.05	0.616	0.17	1.8
1500	100	3.5	105	0.952	100	3.75	112.5	0.888	0.064	0.018	1.77
1480	40	5.5	165	0.242	30	5	150	0.2	0.042	0.012	1.75

*Initial Load

TABLE B21

Load Relaxation Data for 1" Straight Steel Fiber Series

Fiber volume: 0.25%

Load at failure: 920 lb

Load after failure: 580 lb

Apparent Relaxation (a)					Corresponding Background Relaxation (b)				True Relaxation	Velocity	Stress Intensity
load lb p	load lb dp	paper (in) dm	time (sec) dt	slope $(\frac{dp}{dt})_b$	load lb dp	paper (in) dm	time (sec) dt	slope $(\frac{dp}{dt})_a$	$(\frac{dp}{dt})_a - (\frac{dp}{dt})_b$	$V \times 10^{-2}$ in/sec	K ksi-in$^{\frac{1}{2}}$
*720	380	1.5	45	8.44	340	2	60	5.667	2.777	1.5	0.85
700	240	2.5	75	3.2	140	2	60	2.333	0.867	0.51	0.827
680	60	1.875	56.25	1.06	80	3.5	105	0.762	0.304	0.189	0.803
670	30	3	90	0.333	40	4.5	135	0.296	0.037	0.024	0.791
660	20	6.5	195	0.103	20	9	270	0.074	0.029	0.019	0.780

*Initial Load

TABLE B22

Load Relaxation Data for 1" Straight Steel Fiber Series

Fiber volume: 0.5%

Load at failure: 1560 lb

Load after failure: 540 lb

Apparent Relaxation (a)					Corresponding Background Relaxation (b)				True Relaxation	Velocity	Stress Intensity
load lb p	load lb dp	paper (in) dm	time (sec) dt	slope $(\frac{dp}{dt})_b$	load lb dp	paper (in) dm	time (sec) dt	slope $(\frac{dp}{dt})_a$	$(\frac{dp}{dt})_a - (\frac{dp}{dt})_b$	$V \times 10^{-2}$ in/sec	K ksi-in$^{\frac{1}{2}}$
*1300	470	1	30	15.667	300	1	30	10	5.667	1.74	1.535
1280	350	1.5	45	7.778	300	1.938	58.1	5.16	2.616	0.83	1.512
1270	190	1.56	46.88	4.05	210	2	60	3.5	0.553	0.172	1.5
1260	120	1.75	52.5	2.286	180	3.25	97.5	1.846	0.44	0.144	1.488
1240	60	2.375	71.25	0.842	60	2.5	7.5	0.8	0.042	0.014	1.465
1200	20	6	180	0.111	20	8	240	0.083	0.028	0.01	1.417

*Initial Load

TABLE B23

Load Relaxation Data for 1" Straight Steel Fiber Series

Fiber volume: 1.0%

Load at failure: 2000 lb

Load after failure: 1100 lb

Apparent Relaxation (a)					Corresponding Background Relaxation (b)				True Relaxation	Velocity	Stress Intensity
load lb p	load lb dp	paper (in) dm	time (sec) dt	slope $(\frac{dp}{dt})_b$	load lb dp	paper (in) dm	time (sec) dt	slope $(\frac{dp}{dt})_a$	$(\frac{dp}{dt})_a - (\frac{dp}{dt})_b$	$V \times 10^{-2}$ in/sec	K $\frac{1}{2}$ ksi-in
*1200	300	0.5	15	20	358	1.5	45	7.95	12.05	4	1.417
1180	440	1.5	45	9.77	280	2.938	88.1	3.177	6.60	2.27	1.394
1160	290	3	90	3.222	190	4.25	127.5	1.49	1.732	0.618	1.37
1140	120	2.5	75	1.6	60	3.25	97.5	0.615	0.985	0.36	1.346
1120	60	3.25	97.5	0.615	20	3	90	0.222	0.393	0.15	1.322
1110	30	3	90	0.333	20	3	90	0.222	0.111	0.043	1.311
1100	20	6	180	0.111	10	5	150	0.056	0.056	0.022	1.299

*Initial Load

TABLE B24

Load Relaxation Data for 1" Straight Steel Fiber Series

Fiber volume: 1.25%

Load at failure: 1900 lb

Load after failure: 1180 lb

Apparent Relaxation (a)					Corresponding Background Relaxation (b)				True Relaxation	Velocity	Stress Intensity
load lb p	load lb dp	paper (in) dm	time (sec) dt	slope $(\frac{dp}{dt})_b$	load lb dp	paper (in) dm	time (sec) dt	slope $(\frac{dp}{dt})_a$	$(\frac{dp}{dt})_a - (\frac{dp}{dt})_b$	$V \times 10^{-2}$ in/sec	K $\frac{1}{2}$ ksi-in
*1500	500	1	30	16.67	300	1	30	10	6.67	1.8	1.748
1460	200	1	30	6.67	340	3	90	3.778	2.889	0.8	1.724
1459	220	2.5	75	2.93	140	2.5	75	1.867	1.06	0.302	1.713
1430	50	1.25	37.5	1.33	20	0.75	22.5	0.888	0.445	0.129	1.689
1420	40	2.5	75	0.533	60	5	150	0.4	0.133	0.039	1.677
1400	42	6	180	0.233	20	4	120	0.168	0.066	0.020	1.654

*Initial Load

TABLE B25

Load Relaxation Data for 1" Straight Steel Fiber Series

Fiber volume: 1.5%

Load at failure: 1040 lb

Load after failure: 660 lb

Apparent Relaxation (a)					Corresponding Background Relaxation (b)				True Relaxation	Velocity	Stress Intensity
load lb p	load lb dp	paper (in) dm	time (sec) dt	slope $(\frac{dp}{dt})_b$	load lb dp	paper (in) dm	time (sec) dt	slope $(\frac{dp}{dt})_a$	$(\frac{dp}{dt})_a - (\frac{dp}{dt})_b$	$V \times 10^{-2}$ in/sec	K ksi-in$^{\frac{1}{2}}$
*800	160	0.625	18.8	8.53	340	1.81	54.3	6.25	2.28	1.114	0.945
780	220	1.325	40	5.33	180	1.56	46.8	3.84	1.49	0.78	0.92
770	130	1	30	4.5	108	2.50	75	1.44	0.69	0.37	0.91
760	140	2.5	75	1.86	100	4.50	135	0.741	0.42	0.236	0.90
740	120	7	120	0.576	30	3.75	112.5	0.266	0.309	0.181	0.87
730	70	5.5	165	0.424	28	6	180	0.155	0.269	0.16	0.86
720	20	5.5	165	0.121	10	6	180	0.055	0.066	0.04	0.85
[a]1040	660	1	60	22	340	1.81	54.3	6.25	15.75	60	1.22
980	500	1.125	3.38	7.080	180	1.56	46.8	3.84	10.92	50	1.16
940	320	1	60	5.380	108	2.50	75	1.44	6.82	34	1.11
320	320	1.5	45	4.9	100	4.50	13.5	0.741	5.64	29	1.08

*Initial Load

a Final Load

TABLE B26

Load Relaxation Data for Bent Steel Fiber Series

Fiber volume: 0

Load at failure: 1170 lb

Load after failure: 120 lb

Apparent Relaxation (a)					Corresponding Background Relaxation (b)				True Relaxation	Velocity	Stress Intensity
load lb p	load lb dp	paper (in) dm	time (sec) dt	slope $(\frac{dp}{dt})_b$	load lb dp	paper (in) dm	time (sec) dt	slope $(\frac{dp}{dt})_a$	$(\frac{dp}{dt})_a - (\frac{dp}{dt})_b$	$V \times 10^{-2}$ in/sec	K $\frac{1}{2}$ ksi-in
*1170	370	1	30	12.33	420	1.5	45	9.333	3	10.5	1.38
1140	160	1	30	5.33	180	1.5	45	4	1.333	4.9	1.346
1120	80	1.5	45	1.77	150	3.189	95.6	1.56	0.217	0.83	1.320
1100	310	0.875	26.25	10.33	420	1.5	45	9.333	2.47	0.898	1.299
1070	270	1.5	45	6	180	1.5	45	4	2	0.768	1.270
1050	132	1.81	54.3	2.42	150	3.188	95.6	1.56	0.86	0.343	1.240
1040	60	2.5	75	0.80	80	4.5	135	0.59	0.21	0.085	1.228
1030	60	5	150	0.40	30	3	90	0.333	0.067	0.027	1.216

*Initial Load

TABLE B27

Load Relaxation Data for Bent Steel Fiber Series

Fiber volume: 0.25%

Load at failure: 1400 lb

Load after failure: 600 lb

Apparent Relaxation (a)					Corresponding Background Relaxation (b)				True Relaxation	Velocity	Stress Intensity
load lb p	load lb dp	paper (in) dm	time (sec) dt	slope $(\frac{dp}{dt})_b$	load lb dp	paper (in) dm	time (sec) dt	slope $(\frac{dp}{dt})_a$	$(\frac{dp}{dt})_a - (\frac{dp}{dt})_b$	$V \times 10^{-2}$ in/sec	K ksi-in$^{\frac{1}{2}}$
*1190	610	1.75	52.5	11.6	460	1.2	36	7.66	3.95	1.33	1.41
1180	580	2.688	80.6	7.19	230	1.5	45	5.11	2.087	0.713	1.39
1160	260	3.440	103	2.52	40	1	30	1.333	1.188	0.420	1.37
1140	80	3	90	0.888	40	3	90	0.444	0.444	0.163	1.34
1120	60	5.5	165	0.362	20	5	150	0.133	0.23	0.087	1.32

*Initial Load

TABLE B28

Load Relaxation Data for Bent Steel Fiber Series

Fiber volume: 0.5%

Load at failure: 1180 lb

Load after failure: 820 lb

Apparent Relaxation (a)					Corresponding Background Relaxation (b)				True Relaxation	Velocity	Stress Intensity
load lb p	load lb dp	paper (in) dm	time (sec) dt	slope $(\frac{dp}{dt})_b$	load lb dp	paper (in) dm	time (sec) dt	slope $(\frac{dp}{dt})_a$	$(\frac{dp}{dt})_a - (\frac{dp}{dt})_b$	$V \times 10^{-2}$ in/sec	K $\frac{1}{2}$ ksi-in
*1000	340	1	30	11.33	250	1	30	8.333	3	1.2	1.18
980	200	1	30	6.67	180	1.5	45	4	2.67	1.1	1.157
970	90	0.97	29.1	3.096	70	1.5	45	1.553	1.54	0.65	1.15
960	60	2.125	63.8	0.941	40	2.5	75	0.533	0.408	0.177	1.133
940	40	3	90	0.444	10	3.5	105	0.095	0.349	0.156	1.11
920	20	5	150	0.133	10	3.5	105	0.095	0.038	0.018	1.08

*Initial Load

TABLE B29

Load Relaxation Data for Bent Steel Fiber Series

Fiber volume: 0.75%

Load at failure: 1420 lb

Load after failure: 1100 lb

Apparent Relaxation (a)					Corresponding Background Relaxation (b)				True Relaxation	Velocity	Stress Intensity
load lb p	load lb dp	paper (in) dm	time (sec) dt	slope $(\frac{dp}{dt})_b$	load lb dp	paper (in) dm	time (sec) dt	slope $(\frac{dp}{dt})_a$	$(\frac{dp}{dt})_a - (\frac{dp}{dt})_b$	$V \times 10^{-2}$ in/sec	K ksi-in$^{\frac{1}{2}}$
*840	440	1.5	45	9.77	200	1.5	45	4.45	5.33	2.5	0.99
800	400	3.5	105	3.81	120	3.15	94.5	1.27	2.54	1.33	0.94
780	140	2.5	75	1.867	60	3.25	97.5	0.61	1.258	0.695	0.92
760	60	2.5	75	0.8	60	3.25	9715	0.6	0.2	0.116	0.89
740	40	3.75	112.5	0.356	40	8	240	0.167	0.189	0.1	0.87
720	20	6	180	0.111	20	6	180	0.061	0.05	0.03	0.85

*Initial Load

TABLE B30

Load Relaxation Data for Bent Steel Fiber Series

Fiber volume: 1.25%

Load at failure: 1660 lb

Load after failure: 1300 lb

Apparent Relaxation (a)					Corresponding Background Relaxation (b)				True Relaxation	Velocity	Stress Intensity
load lb p	load lb dp	paper (in) dm	time (sec) dt	slope $(\frac{dp}{dt})_b$	load lb dp	paper (in) dm	time (sec) dt	slope $(\frac{dp}{dt})_a$	$(\frac{dp}{dt})_a - (\frac{dp}{dt})_b$	$V \times 10^{-2}$ in/sec	K ksi-in$^{\frac{1}{2}}$
*1380	300	0.906	27.18	11.03	420	1.656	19.69	8.45	1.86	7.5	1.63
1350	210	1.250	37.5	5.6	150	1.75	52.50	2.857	2.743	0.84	1.59
1330	130	2	60	2.17	140	3.90	117	1.196	0.97	0.37	1.57
1320	80	4	120	0.66	40	3.50	105	0.38	0.28	0.089	1.55
1300	20	1.5	45	0.444	40	3.50	105	0.38	0.064	0.021	1.535

*Initial Load

TABLE B31

Load Relaxation Data for Bent Steel Fiber Series

Fiber volume: 2.0%

Load at failure: 2000 lb

Load after failure: 1680 lb

Apparent Relaxation (a)					Corresponding Background Relaxation (b)				True Relaxation	Velocity	Stress Intensity
load lb p	load lb dp	paper (in) dm	time (sec) dt	slope $(\frac{dp}{dt})_b$	load lb dp	paper (in) dm	time (sec) dt	slope $(\frac{dp}{dt})_a$	$(\frac{dp}{dt})_a - (\frac{dp}{dt})_b$	$V \times 10^{-2}$ in/sec	K ksi-in$^{\frac{1}{2}}$
*1200	830	2.312	69.38	11.96	400	2.5	75	5.33	6.631	2.2	1.417
1170	620	3.188	95.60	6.48	380	3.81	114	3.322	3.16	1.1	1.382
1150	210	3	90	2.333	160	3.75	112.5	1.422	0.911	0.33	1.358
1140	120	3.75	112.5	1.06	40	4	120	0.75	0.317	0.117	1.346
1120	60	3.75	112.5	0.533	140	9.5	285	0.491	0.042	0.016	1.32
1100	42	7	210	0.2	40	8	240	0.167	0.033	0.013	1.299
1080	20	7	210	0.095	8	4	120	0.0667	0.0285	0.012	1.27

* Initial Load